

1 **Amplified role of potential HONO sources in O<sub>3</sub> formation in North China Plain during**  
2 **autumn haze aggravating processes**

3 Jingwei Zhang<sup>1\*</sup>, Chaofan Lian<sup>2,3\*</sup>, Weigang Wang<sup>2,3\*</sup>, Maofa Ge<sup>2,3,7</sup>, Yitian Guo<sup>1,4</sup>, Haiyan Ran<sup>1,4</sup>, Yusheng  
4 Zhang<sup>5</sup>, Feixue Zheng<sup>5</sup>, Xiaolong Fan<sup>5</sup>, Chao Yan<sup>6</sup>, Kaspar R. Daellenbach<sup>6</sup>, Yongchun Liu<sup>5</sup>, Markku Kulmala<sup>5,6</sup>,  
5 Junling An<sup>1,4,7\*</sup>

6 1. State Key Laboratory of Atmospheric Boundary Layer Physics and Atmospheric Chemistry (LAPC), Institute of  
7 Atmospheric Physics (IAP), Chinese Academy of Sciences, Beijing 100029, China

8 2. State Key Laboratory for Structural Chemistry of Unstable and Stable Species, Beijing National Laboratory for  
9 Molecular Sciences (BNLMS), CAS Research/Education Center for Excellence in Molecular Sciences, Institute of  
10 Chemistry, Chinese Academy of Sciences, Beijing 100190, China

11 3. [School of Chemical Sciences, University of Chinese Academy of Sciences, Beijing 100049, China](#)

12 4. [College of Earth and Planetary Sciences, University of the Chinese Academy of Sciences, Beijing 100049,](#)  
13 [China](#)

14 5. [Aerosol and Haze Laboratory, Advanced Innovation Center for Soft Matter Science and Engineering, Beijing](#)  
15 [University of Chemical Technology, Beijing, 100029, China](#)

16 6. [Institute for Atmospheric and Earth System Research/Physics, Faculty of Science, P.O. Box 64, 00014](#)  
17 [University of Helsinki, Helsinki, Finland](#)

18 7. [Center for Excellence in Urban Atmospheric Environment, Institute of Urban Environment, Chinese Academy](#)  
19 [of Sciences, Xiamen 361021, China](#)

20 \*Corresponding author: Weigang Wang ([wangwg@iccas.ac.cn](mailto:wangwg@iccas.ac.cn)), Junling An ([anjil@mail.iap.ac.cn](mailto:anjil@mail.iap.ac.cn))

21 \*\*These authors contributed equally.

23 **Abstract:**

24 Co-occurrences of high concentrations of PM<sub>2.5</sub> and ozone (O<sub>3</sub>) have been  
25 frequently observed in haze aggravating processes in the North China Plain (NCP)  
26 over the past few years. Higher O<sub>3</sub> concentrations in hazy days were supposed to be  
27 related to nitrous acid (HONO), but the key sources of HONO enhancing O<sub>3</sub> during  
28 haze aggravating processes remain unclear. We added six potential HONO sources,  
29 i.e., four ground-based (traffic, soil, and indoor emissions, and the NO<sub>2</sub> heterogeneous  
30 reaction on ground surface (Het<sub>ground</sub>)) sources, and two aerosol-related (the NO<sub>2</sub>  
31 heterogeneous reaction on aerosol surfaces (Het<sub>aerosol</sub>) and nitrate photolysis  
32 (Phot<sub>nitrate</sub>)) sources into the WRF-Chem model and designed 23 simulation scenarios

Formatted: Font: 11 pt

Deleted: 6

Deleted: 3

Deleted: 3

Deleted: 4

Deleted: 4

Deleted: 4

Deleted: 5

Deleted: 5

Deleted: 4

Deleted: 4

Deleted: 5

Deleted: 3

Deleted: 6

Formatted: Font: 小五

Deleted: 4

Deleted: 5

Deleted: 6

Formatted: Font: 小五

Deleted: ,

Deleted: and h

Deleted: during

Deleted: , which was explored by us in this study, ,

Deleted: and will be explored in (This studyresearch by using the WRF-Chem model, ...

Deleted: into the WRF-Chem model, which is improved to included ...

Deleted: potential HONO

Deleted: 5

59 [to explore the unclear key sources](#). The results indicate that ground-based HONO  
60 sources producing HONO enhancements showed a rapid decrease with height, while  
61 the NO+OH reaction and aerosol-related HONO sources decreased slowly with height.  
62  $Phot_{\text{nitrate}}$  contributions to HONO concentrations enhanced with aggravated pollution  
63 levels, the enhanced HONO due to  $Phot_{\text{nitrate}}$  in hazy days was about [ten times](#) larger  
64 than in clean days and  $Phot_{\text{nitrate}}$  dominated [daytime](#) HONO sources (~30–70% when  
65 the ratio of the photolysis frequency of nitrate ( $J_{\text{nitrate}}$ ) to gas nitric acid ( $J_{\text{HNO}_3}$ ) equals  
66 30) at higher layers (>800 m). Compared with that in clean days, the  $Phot_{\text{nitrate}}$   
67 contribution to the enhanced daily maximum 8-h averaged [\(DMA8\)](#)  $O_3$  was increased  
68 by over one magnitude during the haze aggravating process.  $Phot_{\text{nitrate}}$  contributed  
69 only ~5% of the surface HONO in daytime with a  $J_{\text{nitrate}}/J_{\text{HNO}_3}$  ratio of 30 but  
70 contributed ~30–50% of the enhanced  $O_3$  near the surface in NCP in hazy days.  
71 Surface  $O_3$  was dominated by volatile organic compounds-sensitive chemistry, while  
72  $O_3$  at higher altitude (>800m) was dominated by  $NO_x$ -sensitive chemistry.  $Phot_{\text{nitrate}}$   
73 had a limited impact on nitrate concentrations (<15%) even with a  $J_{\text{nitrate}}/J_{\text{HNO}_3}$  ratio of  
74 120. The above results suggest [the potential but significant impact of  \$Phot\_{\text{nitrate}}\$  on  \$O\_3\$](#)   
75 [formation, and that](#) more [comprehensive](#) studies [on  \$Phot\_{\text{nitrate}}\$](#)  in the atmosphere are  
76 still needed.

Deleted: one order of magnitude

Formatted: Subscript

Formatted: Subscript

Deleted: field

Deleted: of  $J_{\text{nitrate}}$

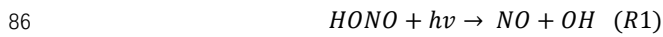
Deleted: nitrate photolysis

Formatted: Subscript

## 78 1. Introduction

79 Nitrous acid (HONO) is an important source of the hydroxyl radical (OH) through

84 its photolysis (R1), and contributes ~20–80% of the primary OH production (Alicke  
85 et al., 2002; Hendrick et al., 2014; Kim et al., 2014).



87 Although it has passed forty years since the first detection of HONO in the  
88 atmosphere (Perner and Platt, 1979), the sources of HONO (especially daytime) and  
89 the dynamic parameters of HONO formation mechanisms are still not well understood  
90 (Ge et al., 2021). The current air quality models with the default gas-phase reaction  
91 (the reverse reaction of R1) always severely underestimate HONO observations,  
92 resulting in low atmospheric oxidation capacity and underestimation of secondary  
93 pollutants like ozone (O<sub>3</sub>) (Li et al., 2010, 2011; Sarwar et al., 2008; Zhang et al.,  
94 2016, 2019a).

Deleted: ,

Deleted: t

95 HONO sources can be generally classified into three categories, i.e., direct  
96 emissions, homogeneous and heterogeneous reactions. Direct emissions are mainly  
97 from traffic (Kramer et al., 2020; Kurtenbach et al., 2001; Liao et al., 2021), soil  
98 (Kubota and Asami, 1985; Oswald et al., 2013; Wu et al., 2019; Xue et al., 2021),  
99 biomass burning (Cui et al., 2021; Rondon and Sanhueza, 1989; Theys et al., 2020)  
100 and indoor combustion processes (Klosterkother et al., 2021; Liu et al., 2019; Pitts et  
101 al., 1985). The reaction of nitric oxide (NO) with OH (Pagsberg et al., 1997; Stuhl and  
102 Niki, 1972) is usually thought as the dominant homogeneous reaction and is important  
103 during daytime but could be neglected at night due to low OH concentrations. Other  
104 minor homogeneous HONO sources including nucleation of NO<sub>2</sub>, H<sub>2</sub>O, and NH<sub>3</sub>  
105 (Zhang and Tao, 2010), via the photolysis of ortho-nitrophenols (Bejan et al., 2006;

Formatted: Subscript

Formatted: Subscript

Formatted: Subscript

108 [Chen et al., 2021; Lee et al., 2016](#)), via the electronically excited  $\text{NO}_2$  and  $\text{H}_2\text{O}$   
109 [\(Crowley and Carl, 1997; Dillon and Crowley, 2018; Li et al., 2008\)](#) and via  
110 [HO<sub>2</sub>·H<sub>2</sub>O+NO<sub>2</sub> reaction \(Li et al., 2015; Li et al., 2014; Ye et al., 2015\)](#). The  
111 heterogeneous reactions mainly include nitrogen dioxide ( $\text{NO}_2$ ) hydrolysis and  
112 reduction reactions on various humid surfaces (Finlayson-Pitts et al., 2003; Ge et al.,  
113 2019; Gómez Alvarez et al., 2014; Ma et al., 2013; Marion et al., 2021; Sakamaki et  
114 al., 1983; Tang et al., 2017; Yang et al., 2021b) and nitrate photolysis ( $\text{Phot}_{\text{nitrate}}$ )  
115 (Romer et al., 2018; [Ye et al., 2016a, b](#); Zhou et al., 2003), and are usually thought as  
116 the main contributors to HONO concentrations in the atmosphere.

117 Among those potential HONO sources, the photolysis of nitrate to produce HONO  
118 in the atmosphere has received extensive attention over the past several years, and the  
119  $\text{Phot}_{\text{nitrate}}$  frequency ( $J_{\text{nitrate}}$ ) is still argued ([Gen et al., 2022](#)). In the laboratory studies,  
120 some researchers (Bao et al., 2018; Ye et al., 2016a, 2017) showed that  $\text{Phot}_{\text{nitrate}}$  was  
121 an important HONO source, the measured  $J_{\text{nitrate}}$  was 1–3 orders larger than the  $J_{\text{gas}}$   
122 nitric acid ( $\text{HNO}_3$ ) photolysis frequency ( $J_{\text{HNO}_3}$ ) and could reach up to  $10^{-4} \text{ s}^{-1}$ , and a  
123 number of substances including humic acid (Yang et al., 2018), sulfate (Bao et al.,  
124 2020) and  $\text{TiO}_2$  (Xu et al., 2021) might enhance the reaction significantly; while Shi et  
125 al. (2021) found that the  $J_{\text{nitrate}}/J_{\text{HNO}_3}$  ratio was  $<10$  when using suspended submicron  
126 particulate sodium and ammonium nitrate rather than  $\text{PM}_{2.5}$  samples. In the field  
127 studies combining with model simulations, Kasibhatla et al. (2018) compared  $\text{NO}_x$   
128 observations in Cape Verde Atmospheric Observatory with GEOS-Chem (Goddard  
129 Earth Observing System-Chemistry) model simulations and reported a  $J_{\text{nitrate}}/J_{\text{HNO}_3}$

Formatted: Font: 小四, Not Italic, Font color: Text 1

Formatted: Subscript

Formatted: Subscript

Formatted: Subscript

Formatted: Subscript

Formatted: Subscript

Formatted: Subscript

Deleted: nitrate photolysis

Formatted: Subscript

Deleted: (Gen et al., 2022)

Deleted: nitrate photolysis

Formatted: Subscript

Deleted: gaseous

134 ratio of 25–50, Romer et al. (2018) reported a  $J_{\text{nitrate}}/J_{\text{HNO}_3}$  ratio of  $< 30$  based on  
135 observations of  $\text{NO}_x$  ( $= \text{NO} + \text{NO}_2$ ) and  $\text{HNO}_3$  over the Yellow Sea and a box model  
136 simulation, while larger  $J_{\text{nitrate}}/J_{\text{HNO}_3}$  ratios (e.g., 300) were inconsistent with the  
137 observed  $\text{NO}_x$  to  $\text{HNO}_3$  ratios. Adopting a  $J_{\text{nitrate}}/J_{\text{HNO}_3}$  ratio of  $\sim 120$  could greatly  
138 improve daytime surface HONO simulations (contributed  $\sim 30$ – $40\%$  of noontime  
139 HONO) by using the Community Multiscale Air Quality model (CMAQ) in the Pearl  
140 River Delta (Fu et al., 2019) or a box model in the Yangtze River Delta (Shi et al.,  
141 2020), while a  $J_{\text{nitrate}}/J_{\text{HNO}_3}$  ratio of 30 produced negligible HONO in clean periods  
142 ( $\sim 2\%$ ) and slightly higher HONO in heavy haze periods ( $\sim 8\%$ ) in the North China  
143 Plain (NCP) by using a box model (Xue et al., 2020) and  $\sim 1\%$  by using CMAQ in  
144 urban Beijing (Zhang et al., 2021). Recently, Zheng et al. (2020) evaluated the effect  
145 of three  $J_{\text{nitrate}}/J_{\text{HNO}_3}$  ratios (1, 10 and 100) on heterogeneous sulfate formation by  
146 using CMAQ and large uncertainties of simulated sulfate concentrations were  
147 reported. The mostly adopted  $J_{\text{nitrate}}/J_{\text{HNO}_3}$  ratios were 1–30 or 100–120 with large  
148 uncertainties, so more efforts are needed to better understand the  $\text{Phot}_{\text{nitrate}}$  impact on  
149 atmospheric oxidation capacity and concentrations of HONO and other secondary  
150 pollutants.  
151 A number of potential HONO sources (e.g., direct emissions,  $\text{NO}_2$  heterogeneous  
152 reactions and  $\text{Phot}_{\text{nitrate}}$ ) have been coupled into several air quality models (An et al.,  
153 2013; Fu et al., 2019; Guo et al., 2020; Li et al., 2010, 2011; Sarwar et al., 2008; Tang  
154 et al., 2015; Xu et al., 2006; Zhang et al., 2019a, 2019b, 2020a, 2021, 2022) to  
155 improve HONO simulations. The improved HONO sources can produce more OH,

Deleted: was

Deleted:

Formatted: Subscript

Formatted: Subscript

Deleted: model

Deleted: ,

Deleted: of nitrate photolysis

Formatted: Subscript

Deleted: HONO concentrations,

Deleted: concentrations

Deleted: nitrate photolysis

Formatted: Subscript

164 which is favorable for the formation of O<sub>3</sub> (Fu et al., 2019; Guo et al., 2020; Li et al.,  
165 2010; Xing et al., 2019; Zhang et al., 2016, 2019a, 2022). O<sub>3</sub> can directly damage  
166 plants and threaten human health (Avnery et al., 2011a, b; Feng et al., 2015, 2019,  
167 [2022](#); Mills et al., 2007, 2018; Richards et al., 1958; Selin et al., 2009; Wilkinson et  
168 al., 2012; [Zhao et al., 2021](#)), an increasing trend of O<sub>3</sub> concentrations in China has  
169 been widely reported in recent years (Chen et al., 2020a; Li et al., 2020; Lu et al.,  
170 2020; Ma et al., 2016; Maji and Namdeo, 2021), [and](#) made O<sub>3</sub> pollution be a severe  
171 concern. A co-occurrence of high PM<sub>2.5</sub> and O<sub>3</sub> concentrations has been frequently  
172 found in China over the past few years, ~~researchers speculated the significant role of~~  
173 HONO in producing O<sub>3</sub> enhancements (Feng et al., 2021; Fu et al., 2019; Tie et al.,  
174 2019; Yang et al., 2021a). ~~Nevertheless, the current knowledge on the HONO~~  
175 difference in O<sub>3</sub> formation during clean and hazy days is still unclear, ~~especially the~~  
176 relative contribution of each potential HONO source to O<sub>3</sub> enhancements during haze  
177 aggravating processes with a co-occurrence of high PM<sub>2.5</sub> and O<sub>3</sub> concentrations.

178 In this study, time series of pollutants including HONO, O<sub>3</sub>, and nitrate were  
179 collected in NCP in Oct.11–31 of 2018, in which high concentrations of PM<sub>2.5</sub>  
180 accompanying by high O<sub>3</sub> concentrations were found at least twice in haze events.  
181 ~~The specific role of each of potential HONO sources in O<sub>3</sub> formation will be explored~~  
182 during these haze events ~~by coupling these potential HONO sources into the Weather~~  
183 ~~Research and Forecasting model with Chemistry (WRF-Chem)~~. The relative  
184 contribution of each potential HONO source to surface-averaged and  
185 vertically-averaged concentrations of HONO and O<sub>3</sub> will be quantified and the

Deleted: and

Deleted: ),

Deleted: but

Deleted: and

Deleted: is still unknown to the best of our knowledge

Deleted: ,

Deleted: thus t

Deleted: coupled into the Weather Research and Forecasting model with Chemistry (WRF-Chem) ...

195 uncertainty in key potential HONO sources (e.g.,  $J_{\text{nitrate}}$ ) will be discussed, in order to  
196 find the key HONO sources resulting in  $\text{O}_3$  enhancements in NCP in different  
197 pollution levels (especially during haze aggravating processes).

## 198 2. Data and methods

### 199 2.1 Observed data

200 The field observation was carried out during October 11–31, 2018, and the  
201 observation site was located in the west campus of Beijing University of Chemical  
202 Technology (BUCT, 116°18'37" E, 39°56'56" N) in Beijing. BUCT is an urban site  
203 close to the third ring road of Beijing, with large human activities, including vehicle  
204 emissions. Instruments were set on the 5<sup>th</sup> floor of the main teaching building. HONO  
205 was measured with a home-made water-based long-path absorption photometer (Chen  
206 et al., 2020b). A dual-channel absorption system was deployed to subtract the  
207 potential interferences, e.g.,  $\text{NO}_2$  hydrolysis. A set of on-line commercial analyzers  
208 (Thermo 48i, 42i, 49i, 43i) was used for measurements of  $\text{CO}$ ,  $\text{NO}_x$ ,  $\text{O}_3$ , and  $\text{SO}_2$ . To  
209 be specific, the 42i used molybdenum  $\text{NO}_2$ -to- $\text{NO}$  converter, there would be a  $\text{NO}_2$   
210 overestimation for the conversion of HONO,  $\text{HNO}_3$ , or other  $\text{NO}_y$ . Considering the  
211 relatively lower concentration compared with  $\text{NO}_2$ , the impact would be minor. The  
212 chemical composition of  $\text{PM}_{2.5}$  was analyzed with a Time-of-Flight Aerosol Chemical  
213 Speciation Monitor (ToF-ACSM, Aerodyne). ToF-ACSM was developed via Fröhlich  
214 et al. (2013) for Non-refractory  $\text{PM}_{2.5}$  measurement. The detailed usage could be  
215 found in Liu et al. (2020), where ionization efficiency calibration of nitrate was

Formatted: Superscript

Formatted: Subscript

Formatted: Subscript

Formatted: Subscript

Formatted: Subscript

Formatted: Subscript

Deleted:

Formatted: Subscript

Formatted: Subscript

217 performed using 300 nm dry NH<sub>4</sub>NO<sub>3</sub> every month during the observation. An online  
218 Single Photon Ionization Time-of-Flight Mass Spectrometer (SPI-ToF-MS, Hexin)  
219 was used for the detection of a large variety of volatile organic compounds (VOCs)  
220 (Gao et al., 2013). Surface observations of O<sub>3</sub>, NO<sub>2</sub>, PM<sub>2.5</sub> and PM<sub>10</sub> at 95 sites in  
221 NCP were obtained from <https://quotsoft.net/air/>, issued by the China Ministry of  
222 Ecology and Environment; surface meteorological observations at 284 sites in NCP  
223 were taken from the National Climatic Data Center, China Meteorological  
224 Administration (**Fig.1**).

Formatted: Subscript

Formatted: Subscript

225 The vertical HONO observations were not available during the Oct.11–31 of 2018  
226 at the BUCT site, we used the observed vertical HONO concentrations from Meng et  
227 al. (2020) in urban Beijing in December of 2016 to evaluate our simulation of vertical  
228 HONO concentrations, which were also used by Zhang et al. (2021) in their CMAQ  
229 evaluation.

Deleted: was

Deleted: at

Deleted: validate

Deleted: model validation

## 231 **2.2 Model description**

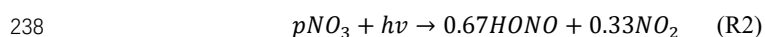
Formatted: Font: (Default) Times New Roman, 小四, Bold, Font color: Text 1

232 The improved WRF-Chem (version 3.7.1), which contained six potential HONO  
233 sources, i.e., traffic (E<sub>traffic</sub>), soil (E<sub>soil</sub>), and indoor (E<sub>indoor</sub>) emissions, Phot<sub>nitrate</sub> in the  
234 atmosphere, and NO<sub>2</sub> heterogeneous reactions on aerosol (Het<sub>aerosol</sub>) and ground  
235 (Het<sub>ground</sub>) surfaces (Zhang et al., 2019a), was used in this study. Phot<sub>nitrate</sub> was newly  
236 added in WRF-Chem (R2) following the work of Fu et al. (2019), Ye et al. (2017),  
237 and Zhou et al. (2003):

Deleted: nitrate photolysis

Formatted: Subscript

Deleted: (Phot<sub>nitrate</sub>)





245 For  $H_{\text{aerosol}}$  and  $H_{\text{ground}}$ , laboratory studies suggest that these heterogeneous  
 246 reactions of  $\text{NO}_2$  to HONO are first order in  $\text{NO}_2$  (Aumont et al., 2003;  
 247 Finlayson-Pitts et al., 2003; Saliba et al., 2000):

- Formatted: Not Superscript/ Subscript
- Formatted: Indent: First line: 0.63 cm
- Deleted: ed
- Formatted: Subscript
- Deleted: is
- Formatted: Subscript



250 The first-order rate constants for aerosol ( $k_a$ ) and ground ( $k_g$ ) surface reactions  
 251 are calculated below:

- Deleted: t
- Formatted: Indent: First line: 0.63 cm

$$k_a = \frac{1}{4} \times v_{\text{NO}_2} \times \left(\frac{S}{V}\right) \times \gamma \quad \text{(E1)}$$

$$k_g = \frac{f \times v_d}{H} \quad \text{(E2)}$$

- Formatted: Centered
- Formatted: Font: Not Italic
- Formatted: Font: Italic

254 where  $v_{\text{NO}_2}$  is the mean molecular speed of  $\text{NO}_2$ ,  $\frac{S}{V}$  is the surface to volume ratio for  
 255 aerosols,  $\gamma$  is the reactive uptake coefficient of aerosols,  $f$  is the proportion of  
 256 deposited  $\text{NO}_2$  reaching the surface in participating HONO formation,  $v_d$  is the dry  
 257 deposition velocity of  $\text{NO}_2$ , and  $H$  is the first model layer height above the ground  
 258 (~35 m). It should be noted that not 100% (50% is commonly accepted) of the  
 259 participated  $\text{NO}_2$  could be converted to HONO in R3 and R4, so  $k_a$  and  $k_g$  were  
 260 multiplied by 0.5 in the final calculation of HONO heterogeneous formation via  $\text{NO}_2$ .

- Deleted: in which
- Deleted: W
- Formatted: Subscript
- Deleted: the
- Formatted: Subscript
- Formatted: Subscript
- Deleted: is the

261 The two factors  $\gamma$  and  $f$  were improved from previous studies (Li et al., 2010; Liu  
 262 et al., 2014; Zhang et al., 2019a) and calculated by:

- Deleted: a production rate of 50% is commonly accepted, and the ...
- Deleted: y
- Deleted: for
- Formatted: Subscript

$$\gamma = 5 \times 10^{-6} \times \left(1 + \frac{\text{SR}}{\alpha}\right) \quad \text{(E3)}$$

$$f = 0.08 \times \left(1 + \frac{\text{SR}}{\alpha}\right) \quad \text{(E4)}$$

- Deleted: The uptake coefficient ( $\gamma$ ) of  $\text{NO}_2$  on aerosol surfaces, and the yield ( $f$ ) of HONO from  $\text{NO}_2$  reaching the ground surfaceThe
- Deleted: R3
- Deleted: R4

265 where SR denotes solar radiation ( $\text{W m}^{-2}$ ),  $\alpha$  is an adjusted parameter and set as 100  
 266 ( $\text{W m}^{-2}$ ), thus  $\gamma$  and  $f$  became continuous functions during the whole day ( $\gamma$  and  $f$

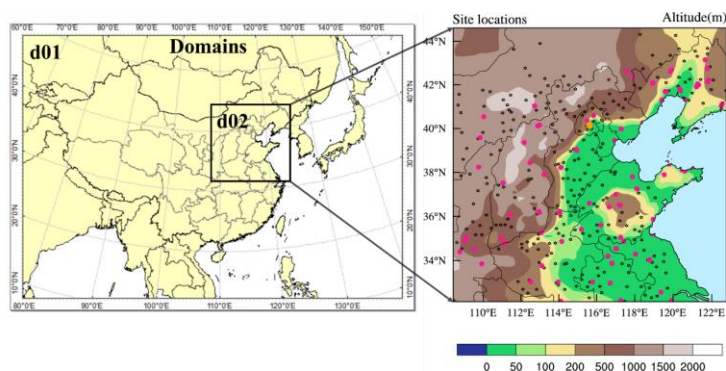
- Formatted: Superscript

283 enhanced by ten times and reached  $5 \times 10^{-5}$  and 0.8 when SR reached  $900 \text{ W m}^{-2}$  at  
284 noontime, respectively).

Deleted: one order of magnitude

Deleted:

285 The physical and chemical schemes used in this study are given in **Table 1**. Two  
286 domains were adopted, domain one contains  $82 \times 64$  grid cells with a horizontal  
287 resolution of 81 km, domain two contains  $51 \times 51$  grid cells with a horizontal  
288 resolution of 27 km (**Fig.1**), both with 17 vertical layers encompassing from the  
289 surface to 100 hPa. The observational sites are shown in the right panel of **Fig.1**,  
290 including one HONO observation site (the orange dot in urban Beijing), 95  
291 observation sites of  $\text{PM}_{2.5}$ ,  $\text{NO}_2$  and  $\text{O}_3$  (pink dots) and 284 meteorological monitoring  
292 sites (black dots).



293  
294 **Figure 1** Domains of WRF-Chem used in this study (left panel), and the locations of one HONO  
295 observation site (the orange dot in urban Beijing), 95 environmental monitoring ( $\text{PM}_{2.5}$ ,  $\text{NO}_2$  and  
296  $\text{O}_3$ ) sites (deep pink dots), and 284 meteorological observation sites (black dots) in domain 2 (right  
297 panel).

298

299 The anthropogenic emissions in East Asia in 2010 were taken from the MIX

302 emission inventory (Li et al., 2017) (<http://www.meicmodel.org/>), including both  
303 gaseous and aerosol species, i.e., SO<sub>2</sub>, NO<sub>x</sub>, CO, VOCs, NH<sub>3</sub>, PM<sub>10</sub>, PM<sub>2.5</sub>, BC, OC  
304 and CO<sub>2</sub>, and were provided monthly by five sectors (power, industry, residential,  
305 transportation, and agriculture) at a resolution of 0.25° × 0.25°. VOC emissions were  
306 speciated into model-ready inputs according to the MOZART chemical mechanism to  
307 build the WRF-Chem emission files. The anthropogenic emissions in China were  
308 replaced by employing the MEIC 2016 (the Multi-resolution Emission Inventory for  
309 China) developed by Tsinghua University. The NH<sub>3</sub> emissions in China were from  
310 Dong et al. (2010), biomass burning emissions were from Huang et al. (2012) and  
311 biogenic emissions were calculated using the Model of Emissions of Gases and  
312 Aerosols from Nature (MEGAN) (Guenther et al., 2012). Due to the sharp reduction  
313 of anthropogenic emissions in recent years, the default emission inventory was  
314 systematically overestimated in autumn of 2018, especially for SO<sub>2</sub> and PM<sub>2.5</sub>  
315 concentrations. Based on the comparison of simulations and observations (the urban  
316 Beijing site plus other 95 pollutant monitoring sites in NCP), we cut off 80% of SO<sub>2</sub>  
317 emissions, 50% of NH<sub>3</sub> emissions, 30% of toluene emissions, and 50% of PM<sub>2.5</sub> and  
318 PM<sub>10</sub> emissions. The cut-off emissions are largely close to the emission reductions in  
319 east China during 2013 to 2017 (Zhang and Geng, 2019). The revised emissions  
320 significantly improved regional PM<sub>2.5</sub> simulations in NCP (**Fig.S1**), and the  
321 simulations of gases and PM<sub>2.5</sub> in urban Beijing (**Fig.S2**).

322 The National Centers for Environmental Prediction (NCEP) 1° × 1° final  
323 reanalysis data (FNL) (<https://rda.ucar.edu/datasets/ds083.2/>) were used in this study

324 to obtain the meteorological initial and boundary conditions every 6 h. The global  
 325 simulations of MOZART-4 (<https://www.acom.ucar.edu/wrf-chem/mozart.shtml>)  
 326 were used as the chemical initial and boundary conditions (every 6 h).

327

328 **Table1** Physical and chemical options in WRF-Chem used in this study

Options	WRF-Chem
Advection scheme	Runge-Kutta 3 <sup>rd</sup> order
Boundary layer scheme	YSU
Cloud microphysics	Lin et al. (1983)
Cumulus parameterization	New Grell scheme
Land-surface model	Noah
Long-wave radiation	RRTM
Short-wave radiation	Goddard
Surface layer	Revised MM5 Monin-Obukhov scheme
Aerosol option	MOSAIC ( <a href="#">Zaveri et al., 2008</a> )
Chemistry option	Updated MOZART mechanism ( <a href="#">Emmons et al., 2010</a> )
Photolysis scheme	F-TUV

329

330 Totally 23 simulation scenarios were performed in this study (**Table 2**), in which  
 331 the base case only considered the default homogeneous reaction ( $\text{OH} + \text{NO} \rightarrow$   
 332  $\text{HONO}$ ), case 6S contained six potential HONO sources while case A, B, C, D, E and  
 333 F contained each of the six potential HONO sources, respectively. Other 15 cases  
 334 (A\_double, A\_half, ..., Nit\_120, D\_NO<sub>2</sub> and D\_HONO) were used to evaluate the  
 335 uncertainties of the six potential HONO sources (**Table 2**). All of the cases were  
 336 simulated with a spin-up of 7 days.  $J_{\text{nitrate}}$  and  $J_{\text{HNO}_3}$  denote the photolysis frequency of  
 337 nitrate and gas nitric acid in the atmosphere, respectively. ~~The~~ enhancement factor for  
 338 F\_double was 1.25 rather than 2.0 to avoid the production rate of HONO from NO<sub>2</sub>  
 339 reaching the surface exceeding 100%. ~~The~~ 0.33NO<sub>2</sub> in D NO<sub>2</sub> or 0.67HONO in  
 340 D\_HONO referred to the assumed  $\text{Phot}_{\text{nitrate}}$  products in R2.

Formatted: Superscript

Deleted: ;

Deleted: the

Deleted: %,

Deleted: while

Formatted: Subscript

Deleted: of the nitrate photolysis

Deleted: The c

347

348 **Table 2.** Simulation scenarios designed in this study.

Case	HONO sources
Base	Default (OH + NO → HONO)
6S	Default + E <sub>traffic</sub> + E <sub>soil</sub> + E <sub>indoor</sub> + Phot <sub>nitrate</sub> (J <sub>nitrate</sub> /J <sub>HNO3</sub> = 30) + Het <sub>aerosol</sub> + Het <sub>ground</sub>
A	Default + E <sub>traffic</sub>
B	Default + E <sub>soil</sub>
C	Default + E <sub>indoor</sub>
D	Default + Phot <sub>nitrate</sub> (J <sub>nitrate</sub> /J <sub>HNO3</sub> = 30)
E	Default + Het <sub>aerosol</sub>
F	Default + Het <sub>ground</sub>
A_double	Default + 2×E <sub>traffic</sub>
A_half	Default + 0.5×E <sub>traffic</sub>
B_double	Default + 2×E <sub>soil</sub>
B_half	Default + 0.5×E <sub>soil</sub>
C_double	Default + 2×E <sub>indoor</sub>
C_half	Default + 0.5×E <sub>indoor</sub>
E_double	Default + Het <sub>aerosol</sub> (2×γ)
E_half	Default + Het <sub>aerosol</sub> (0.5×γ)
F_double	Default + Het <sub>ground</sub> (1.25×f)
F_half	Default + Het <sub>ground</sub> (0.5×f)
Nit_1	Default + Phot <sub>nitrate</sub> (J <sub>nitrate</sub> /J <sub>HNO3</sub> = 1)
Nit_7	Default + Phot <sub>nitrate</sub> (J <sub>nitrate</sub> /J <sub>HNO3</sub> = 7)
Nit_120	Default + Phot <sub>nitrate</sub> (J <sub>nitrate</sub> /J <sub>HNO3</sub> = 120)
D_NO2	Only 0.33NO <sub>2</sub> produced in Phot <sub>nitrate</sub> for case D
D_HONO	Only 0.67HONO produced in Phot <sub>nitrate</sub> for case D

349 **3.Results**

350 **3.1 Comparison of simulations and observations**

351 **3.1.1 Meteorological factors**

352 The statistical metrics of simulated meteorological parameters at 284 sites in NCP  
 353 including air temperature (T), relative humidity (RH) and wind speed (WS) were  
 354 comparable with the previous modelling results of other researchers (Table 3). The  
 355 simulated wind direction (WD) bias within 45° accounted for ~56%, and the bias  
 356 within 90° accounted for ~80%, suggesting that the simulated WD captured the main  
 357 observed WD.

Deleted: ,

Deleted: the

360

361 **Table 3.** Performance metrics (index of agreement (IOA), RMSE (root-mean-square error)  
362 and MB (mean bias)) of WRF-Chem simulated air temperature, relative humidity, wind speed and  
363 direction at 284 meteorological sites in the North China Plain during Oct. 11–31 of 2018. The  
364 definitions of the metrics used in this study are given in Text S1.

Deleted: is

	IOA	RMSE	MB	Reference
<b>T (°C)</b>	<b>0.97</b>	<b>1.4</b>	<b>-1.1</b>	<b>This work</b>
	0.90	2.5	0.2	(Wang et al., 2014)
	0.90	/	-0.9	(Wang et al., 2010)
	0.88	/	0.5	(Li et al., 2012)
	/	3.1	0.8	(Zhang et al., 2012)
<b>RH (%)</b>	<b>0.90</b>	<b>9.0</b>	<b>-7.1</b>	<b>This work</b>
	0.78	16.3	-5.5	(Wang et al., 2014)
	0.78	/	-1.3	(Wang et al., 2010)
	0.86	/	-1.1	(Li et al., 2012)
	/	17.4	-5.7	(Zhang et al., 2012)
<b>WS (m s<sup>-1</sup>)</b>	<b>0.48</b>	<b>1.4</b>	<b>1.3</b>	<b>This work</b>
	0.56	2.5	1.6	(Wang et al., 2014)
	0.65	2.1	0.9	(Wang et al., 2010)
	0.62	1.5	0.6	(Li et al., 2012)
	/	2.2	1.1	(Zhang et al., 2012)
<b>WD Bias</b>	<i>0-45°</i>	<i>45-90°</i>	<i>&gt;90°</i>	
<b>Count</b>	<i>75701</i>	<i>21500</i>	<i>28075</i>	<i>135276(Total)</i>
<b>Percentage</b>	<b>55.96%</b>	<b>23.29%</b>	<b>20.75%</b>	

### 365 3.1.2 Pollutant concentrations at the BUCT site

366 Time series of the observational data at the BUCT site are shown in Fig.2, the  
367 gray shaded periods stand for three haze aggravating processes, while the cyan shaded  
368 period denotes typical clean days, respectively. The hourly largest observations of O<sub>3</sub>  
369 (~50–75 ppb) and PM<sub>2.5</sub> (~100–200 µg/m<sup>3</sup>) were both relatively higher in hazy days  
370 than in clean days, especially for the first two haze events (the O<sub>3</sub> concentrations in  
371 the third haze event was relatively lower due to the higher NO<sub>x</sub> concentrations in the  
372 urban area).

373 The observed PM<sub>2.5</sub> and nitrate trends at the BUCT site were well simulated

375 (Fig.2a&b), and NO<sub>2</sub> simulations generally agreed with the observations (Fig.2c).

376 ~~The promotion effect of the six potential HONO sources on the formation of~~  
377 ~~secondary aerosols leads to an increase in concentrations of PM<sub>2.5</sub> and nitrate for case~~  
378 ~~6S, despite nitrate consumption through Phot<sub>nitrate</sub> (Li et al., 2010; Qu et al., 2019; Fu~~  
379 ~~et al., 2019; Zhang et al., 2019a, 2021), detailed nitrate variation caused by each of~~  
380 ~~the six potential HONO sources in case 6S is presented in Fig.S3. Hourly and diurnal~~  
381 HONO simulations at the BUCT site (Fig.2d&3a) were significantly improved in the  
382 6S case (mean is 1.47 ppb) compared with the base case (mean is 0.05 ppb). The  
383 normalized mean bias (NMB) was remarkably reduced to -14.22% (6S) from -97.11%  
384 (Base), and the index of agreement (IOA) was improved significantly to **0.80 (6S)**  
385 ~~from 0.45 (Base), (Fig.2d). The underestimation of the simulated HONO (6S) on~~  
386 ~~Oct.15 and Oct.22 was mainly caused by the earlier scavenging of pollutants at the~~  
387 ~~BUCT site in the used model (Fig.2a&d).~~

388 As for O<sub>3</sub>, noticeable improvements could be found at the BUCT site after  
389 considering the six potential HONO sources, especially in hazy days (Fig.2e&f). The  
390 mean bias (MB) was improved to -3.61 ppb (6S) from -7.09 ppb (Base), and the IOA  
391 was improved to **0.86 (6S) from 0.78 (Base)**, (Fig.2e). Specially, the 6S case  
392 significantly enhanced daytime hourly O<sub>3</sub> by 15–35 ppb compared with the base case  
393 and the simulated O<sub>3</sub> was very close to the observations in hazy days (Fig.2e). Larger  
394 daytime O<sub>3</sub> enhancements were accompanied with higher PM<sub>2.5</sub> concentrations during  
395 haze aggravating processes, while in clean days the daytime enhanced O<sub>3</sub> due to the  
396 potential HONO sources was mostly < 5 ppb (Fig.2e&f). The diurnal O<sub>3</sub> pattern

Deleted: The increased PM<sub>2.5</sub> and nitrate concentrations for 6S case was because of the ...

Deleted: additional

Deleted: formation

Formatted: Subscript

Deleted: the

Deleted: of nitrate

Deleted: nitrate photolysis

Formatted: Subscript

Deleted: given

Formatted: Font: Bold

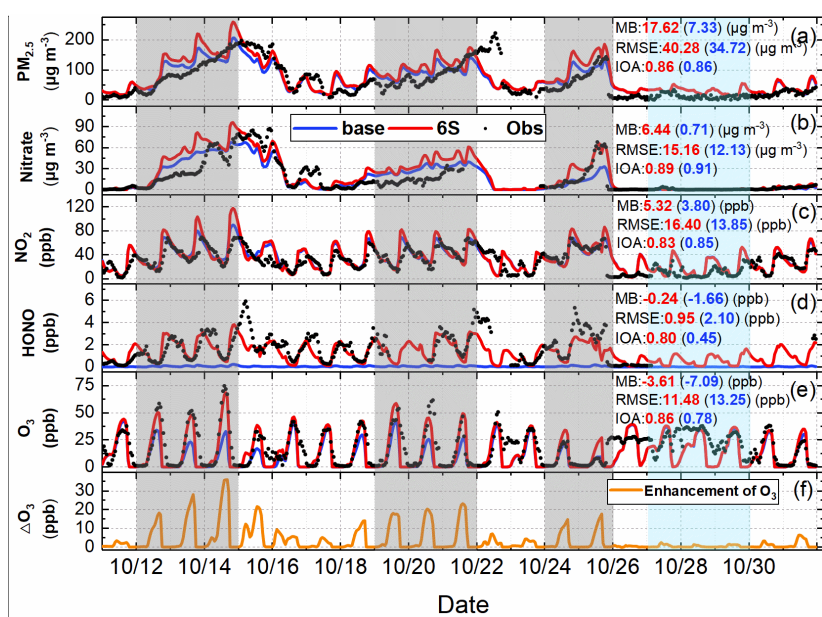
Deleted: 0.86 (6S) from 0.78 (Base)

Formatted: Font: Bold

Deleted: .

Deleted: 0.80 (6S) from 0.45 (Base)

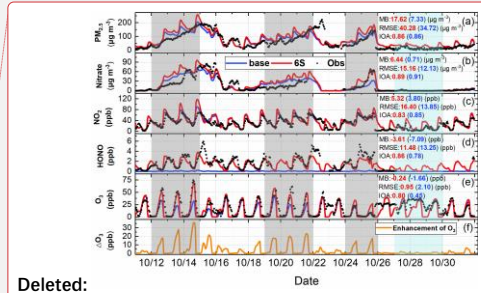
408 during the first two haze aggravating processes is presented in **Fig.3b**, significant  
 409 improvements in daily maximum 8-h (10:00–17:59) averaged (DMA8) O<sub>3</sub> (18.8 ppb)  
 410 occurred at the BUCT site after considering the six potential HONO sources, and the  
 411 NMB of DMA8 O<sub>3</sub> was remarkably improved to -2.38% (6S) from -47.14% (Base).  
 412



413  
 414 **Figure 2** Comparison of simulated (Base and 6S cases) and observed hourly concentrations of  
 415 PM<sub>2.5</sub>, nitrate, NO<sub>2</sub>, HONO and O<sub>3</sub> (a–e), and the hourly enhanced concentrations of O<sub>3</sub> (ΔO<sub>3</sub>) (f)  
 416 caused by the six potential HONO sources (6S minus Base) at the BUCT site during Oct.11–31 of  
 417 2018.

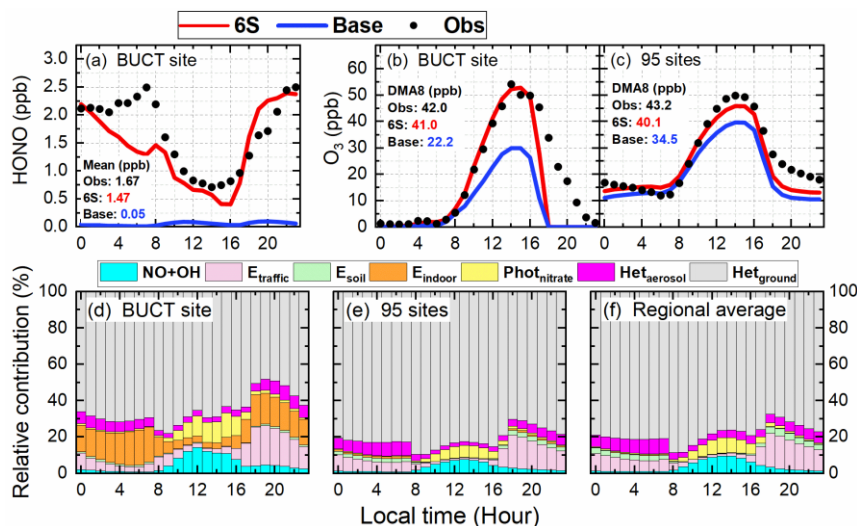
418  
 419

**Commented [j1]:** The statistics for O<sub>3</sub> and HONO was opposite in the original figure, which is corrected now. For the orders of panel O<sub>3</sub> and HONO was swapped previously to let O<sub>3</sub> next to ΔO<sub>3</sub>, but the statistics was forgotten to change the orders simultaneously.



Deleted:





421

422 **Figure 3** Comparison of diurnal mean simulations (Base and 6S cases) and observations of  
 423 HONO during the study period (a) and O<sub>3</sub> during the first two haze events at the BUCT site (b),  
 424 and O<sub>3</sub> averages at the 95 NCP monitoring sites during the study period (c); and the relative  
 425 contributions of each of the six potential HONO sources and the reaction of OH with NO to  
 426 surface HONO concentrations for the 6S case at the BUCT site (d), at the 95 monitoring sites (e)  
 427 and in the whole NCP region (f). (The calculated 24-h mean HONO concentrations and DMA8 O<sub>3</sub>  
 428 concentrations were given in panels (a) – (c)).

429

430 The relative contribution of each HONO source near the surface at the BUCT site  
 431 for the 6S case is shown in **Fig.3d**. Briefly, Het<sub>ground</sub> was the largest source during  
 432 daytime and nighttime (~50–70%), consistent with the results of Zhang et al. (2021).  
 433 Phot<sub>nitrate</sub> ( $J_{\text{nitrate}}/J_{\text{HNO}_3} = 30$ ) and the NO+OH reaction contributed similarly ~1–12%  
 434 during daytime. E<sub>traffic</sub> was important during nighttime (~10–20%) but small during  
 435 daytime (<5%). The contribution of Het<sub>aerosol</sub> to HONO concentrations was minor

Deleted: .

Formatted: Font: Not Bold

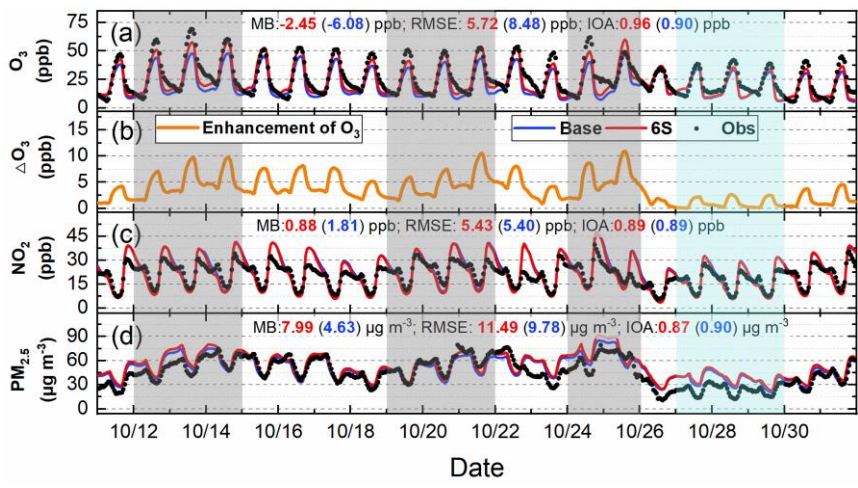
437 (~2–3%) in daytime and ~6–10% in nighttime.  $E_{\text{soil}}$  could be neglected while the  
438 contribution of  $E_{\text{indoor}}$  was close to that of  $E_{\text{traffic}}$  in urban Beijing. The relative  
439 contribution of the potential HONO sources in this study was comparable with the  
440 result of Fu et al. (2019) by using CMAQ, except for the contribution of  $\text{Phot}_{\text{nitrate}}$  due  
441 to the different  $J_{\text{nitrate}}/J_{\text{HNO}_3}$  ratios (30 in our study and ~120 in Fu et al. (2019)).

442

### 443 3.1.3 Pollutant concentrations in NCP

444 The 95-site-averaged hourly simulations and observations of  $\text{O}_3$ ,  $\text{NO}_2$  and  $\text{PM}_{2.5}$   
445 during the study period are shown in **Fig.4**. The six potential HONO sources  
446 significantly improved hourly  $\text{O}_3$  simulations, remarkably enhanced the daily  
447 maximum  $\text{O}_3$  by ~5–10 ppb during Oct. 11–25, and by ~2–4 ppb during Oct. 26–31  
448 (**Fig.4a&b**). The simulations of  $\text{NO}_2$  well agreed with the observations, and the mean  
449 concentrations were 22.55 (Base), 21.62 (6S) and 20.74 (Obs) ppb (**Fig.4c**). The  
450  $\text{PM}_{2.5}$  simulations generally followed the observed  $\text{PM}_{2.5}$  trend but were  
451 overestimated by ~8  $\mu\text{g m}^{-3}$ , with averaged concentrations of 49.94 (Base), 53.30 (6S)  
452 and 45.31 (Obs)  $\mu\text{g m}^{-3}$  (**Fig.4d**), respectively.

453



454

455 **Figure 4** Comparison of 95-site-averaged hourly simulations (Base and 6S cases) and observations of  
 456 O<sub>3</sub>(a), NO<sub>2</sub> (c) and PM<sub>2.5</sub> (d), and O<sub>3</sub> enhancements due to the six potential HONO sources (6S minus  
 457 Base case) (b) in the North China Plain during Oct.11–31 of 2018.

458

459 The 95-site-averaged diurnal simulations and observations of O<sub>3</sub> are presented in  
 460 **Fig.3c**, O<sub>3</sub> simulations showed a remarkable improvement when the six potential  
 461 HONO sources were considered, the six potential HONO sources produced a mean  
 462 enhancement of 5.7 ppb in DMA8 O<sub>3</sub> and improved the NMB to -7.16% from -20.32%  
 463 at the 95 sites in NCP. The 95-site-averaged diurnal simulations and observations of  
 464 NO<sub>2</sub> and PM<sub>2.5</sub> during the study period are demonstrated in **Fig.S4**. NO<sub>2</sub> simulations  
 465 generally followed the observed trend but were underestimated during 04:00 to 16:00  
 466 and overestimated after 18:00 (**Fig.S4a**), PM<sub>2.5</sub> simulations agreed with the observed  
 467 diurnal pattern but were overestimated for both cases during the whole day (**Fig.S4b**).

468 The relative contribution of each HONO source near the surface at the 95 NCP  
 469 sites for the 6S case is shown in **Fig.3e**. Het<sub>ground</sub> was the dominant source during

Deleted: mean  
 Deleted: simulated  
 Deleted: observed hourly

Deleted: (10:00–17:59)  
 Deleted: from -20.32%

Deleted: S3

Deleted: S3a

Deleted: S3b

478 daytime and nighttime (~70–80%).  $Phot_{nitrate}$  ( $J_{nitrate}/J_{HNO_3} = 30$ ) and the NO+OH  
479 reaction nearly equaled and contributed ~2–8% during daytime (~5% on average).  
480  $E_{traffic}$  was important during nighttime (~10–15%) but small during daytime (<3%).  
481 The contribution of  $Het_{aerosol}$  to HONO concentrations was <3% in daytime and <10%  
482 in nighttime.  $E_{soil}$  contributed ~3% in nighttime but could be neglected in daytime.  
483 The contribution of  $E_{indoor}$  was too small to be noticed at the 95 NCP sites, implying  
484 that this source was noticeable only in megacities. The relative contribution of each  
485 HONO source in the whole NCP region (all grid cells in domain two except for the  
486 seas) is presented in **Fig.3f**, the results were quite similar with those at the 95 sites  
487 (**Fig.3f**), [which](#) were representative for the whole NCP region. To further understand  
488 the role of potential HONO sources in haze aggravating processes in regional  $O_3$   
489 concentrations, the 95 site-averaged surface/vertical HONO concentrations and their  
490 impacts during a typical haze event (Oct. 19–21) and a clean period (Oct. 27–29) were  
491 analyzed and [are](#) shown in the following sections.

Formatted: Font: 小四

Deleted: thus the results of the 95 sites

## 493 3.2 Spatial distribution of enhanced DMA8 $O_3$ by potential HONO sources

### 494 3.2.1 General patterns of enhanced DMA8 $O_3$

495 **Fig.S5** shows surface-averaged and zonal-averaged DMA8  $O_3$  enhancements due  
496 to the six potential HONO sources in NCP during the study period (Oct.11-31) and  
497 three haze events (Oct.12–14, Oct.18–21 and Oct.24–25). The overall surface DMA8  
498  $O_3$  enhancement decreased gradually from south (6–10 ppb) to north (2–6 ppb)

Deleted: S4

Deleted: ly

502 (Fig.S5a) and could reach 10–20 ppb under unfavorable meteorological conditions  
503 during haze events (Fig.S5b–d). For the first two haze events, the anti-cyclone in the  
504 Shandong peninsula carried pollutants being transported from the southeastern NCP  
505 to the western (108–112°E) and northern (39–41°N) NCP, and the six potential  
506 HONO sources led to a DMA8 O<sub>3</sub> enhancement of 10–20 ppb (Fig.S5b) and 10–15  
507 ppb (Fig.S5c) in Beijing, respectively. For the third haze event, two air masses were  
508 converged to form a transport channel from south to north, the O<sub>3</sub> enhancement  
509 caused by the six potential HONO sources can reach 10–18 ppb in the southern NCP  
510 and decreased to 6–10 ppb in the northern NCP along the transport channel. Vertically,  
511 the DMA8 O<sub>3</sub> enhancements were 2–8 ppb during the whole period (Fig.S5e) and  
512 increased to 6–12 ppb in these haze events (Fig.S5f–h). The enhanced O<sub>3</sub> near the  
513 surface (0–100 m) was slightly smaller than that at higher altitude (Fig.S5f–h), due  
514 mainly to the stronger titration of O<sub>3</sub> by NO near the surface. The above results  
515 demonstrated that the six potential HONO sources significantly enhanced surface and  
516 vertical O<sub>3</sub> concentrations in NCP, especially during haze events.

Deleted: S4a

Deleted: S4b

Deleted: S4b

Deleted: S4c

Deleted: S4e

Deleted: S4f

Deleted: S4f

517

### 518 3.2.2 During a typical haze aggravating process and a clean period

519 Fig.5 demonstrates surface-averaged and zonally-averaged DMA8 O<sub>3</sub>  
520 enhancements due to the six potential HONO sources in NCP during a typical haze  
521 aggravating process (Oct.19–21, 2018) and a clean period (Oct.27–29, 2018). The  
522 increasing trend of DMA8 O<sub>3</sub> enhancements can be clearly seen from Oct.19 to

530 Oct.21 near the surface and in the vertical direction. During the haze aggravating  
 531 process, the surface DMA8 O<sub>3</sub> enhancements were ~2–10 ppb (Oct.19), ~6–12 ppb  
 532 (Oct.20) and ~8–15 ppb (Oct.21), respectively. ~~the~~ vertical DMA8 O<sub>3</sub> enhancements  
 533 were ~4–7 ppb (Oct.19), ~6–10 ppb (Oct.20), and ~8–15 ppb (Oct.21), respectively. ~~;~~  
 534 While during clean days, the surface/vertical DMA8 O<sub>3</sub> enhancements were usually  
 535 <4 ppb. The six potential HONO sources significantly enhanced surface and vertical  
 536 O<sub>3</sub> concentrations in NCP during haze aggravating processes, the detailed role of the  
 537 potential HONO sources on vertical HONO concentrations and their impacts are  
 538 presented in the next section.

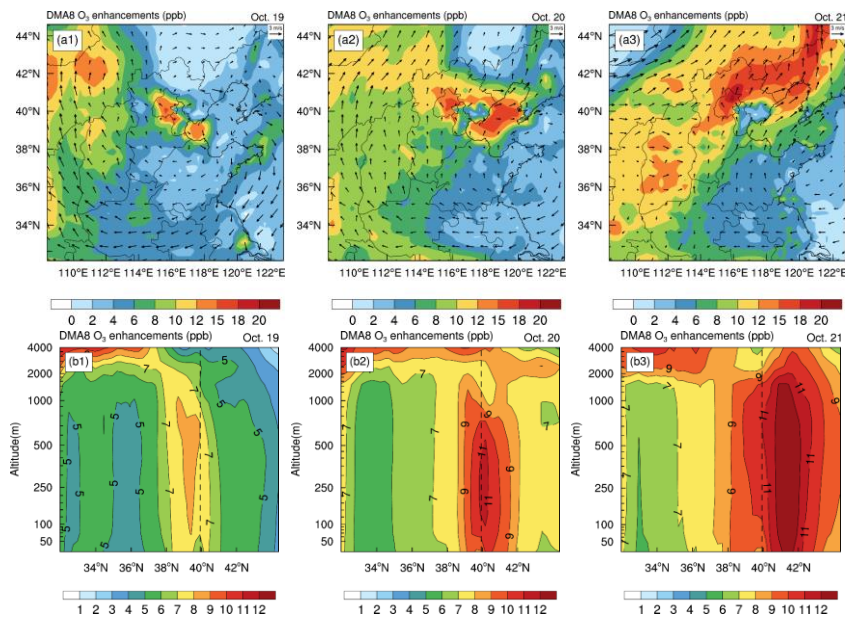
Deleted: , and

Deleted: ;

Deleted: while

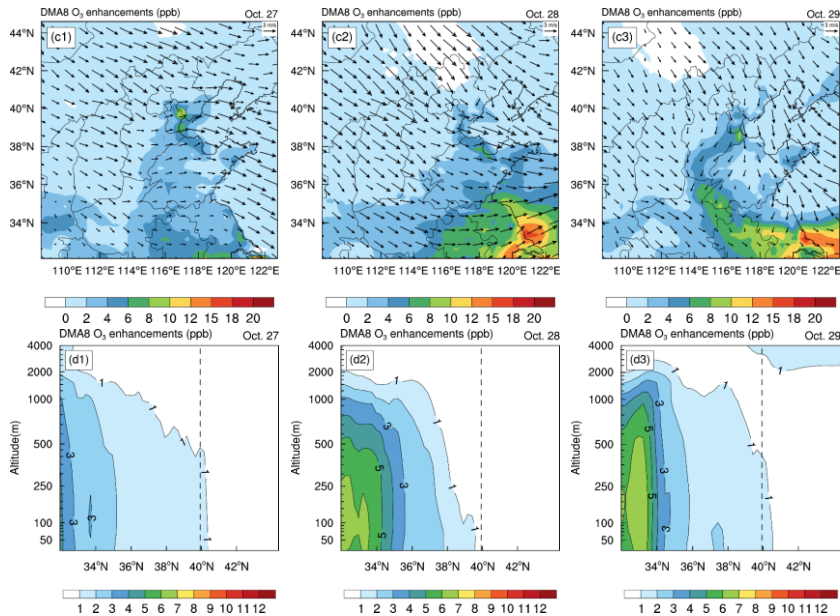
Deleted: were given

539



540

541



546

547

548

549

550

551

552

553

554

555

556

557

558

**Figure 5** Surface-averaged (a1–a3, c1–c3) and zonal-averaged (b1–b3, d1–d3) DMA8 O<sub>3</sub> enhancements due to the six potential HONO sources in the North China Plain during a typical haze aggravating process (Oct.19–21, 2018) and a clean period (Oct.27–29, 2018). (The dashed line denotes the latitude of the BUCT site).

Deleted: ly

Deleted: .

### 3.3 Vertical variations of [the six](#) potential HONO sources and their impacts

#### 3.3.1 [Six potential](#) HONO sources and their impacts on HONO concentrations

Deleted: Potential

A number of studies have conducted vertical HONO observations abroad (Kleffmann et al., 2003; Ryan et al., 2018; Sorgel et al., 2011; VandenBoer et al., 2013; Villena et al., 2011; Wang et al., 2020; Wong et al., 2011, 2012; Zhang et al., 2009) and in China (Meng et al., 2020; Wang et al., 2019; Xing et al., 2021; Zhu et al., 2011).

Deleted: ),

563 A decreasing trend of HONO with height was mostly observed among these studies,  
564 and our simulations also reproduced this vertical variation and were comparable with  
565 another model simulation by Zhang et al. (2021) who used CMAQ (Fig.S6). For a  
566 deep understanding of the role of each considered HONO source in HONO  
567 concentrations at different heights, we assessed the contributions of each potential  
568 HONO source to HONO concentrations at different heights (Fig.6) during Oct.11–31  
569 of 2018.

Deleted: a

Deleted: whom using the

Deleted: model

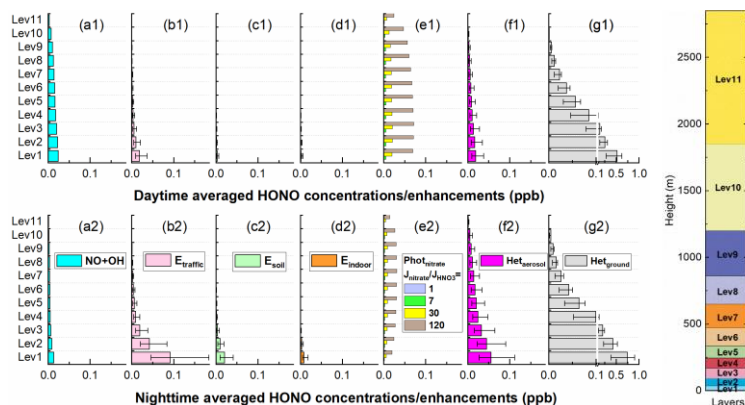
Deleted: S5

570 Generally, the impacts of ground-based potential HONO sources ( $E_{\text{traffic}}$ ,  $E_{\text{soil}}$ ,  
571  $E_{\text{indoor}}$  and  $H_{\text{etground}}$ ) on HONO concentrations decreased rapidly with height, while  
572 the NO+OH reaction and aerosol related HONO sources ( $Phot_{\text{nitrate}}$  and  $H_{\text{et aerosol}}$ )  
573 decreased slowly with height (Fig.6). During daytime the NO+OH reaction,  $Phot_{\text{nitrate}}$   
574 and  $H_{\text{etground}}$  were the three main HONO sources, while during nighttime  $E_{\text{traffic}}$ ,  
575  $H_{\text{et aerosol}}$  and  $H_{\text{etground}}$  were the three main contributors to HONO concentrations  
576 (Fig.6). The HONO concentrations via the NO+OH reaction and  $Phot_{\text{nitrate}}$  were  
577 higher during daytime. The impact of  $E_{\text{soil}}$  in the NCP was small, nevertheless, Xue et  
578 al. (2021) found strong soil HONO emissions in NCP agricultural fields after  
579 fertilization, suggesting that this source may have a remarkable enhancement on  
580 regional HONO and secondary pollutants in crop growing seasons.

Deleted: however

581





587  
 588 **Figure 6** The 95-site-averaged daytime/nighttime HONO concentrations/enhancements at  
 589 different heights when the NO+OH reaction (a1&a2) and each of the six potential HONO sources  
 590 (b1–g1&b2–g2) were considered during Oct.11–31 of 2018. (The error bar denotes the  
 591 uncertainties of each potential HONO source in HONO concentrations (Table 2). The right panel  
 592 denotes the approximate height of each vertical layer above the ground).

Deleted: ,  
 Deleted: the

593  
 594 The comparison of HONO concentrations/enhancements during a haze  
 595 aggravating process and a clean period is shown in Figs.7&8. Generally, daytime  
 596 HONO concentrations increased in haze aggravating processes and were higher than  
 597 those in clean days. Het<sub>ground</sub> was the dominant source of the surface HONO in both  
 598 hazy and clean days and contributed 80–90% of daytime averaged HONO  
 599 concentrations (Fig.8), however, this reaction occurred only on the ground surface,  
 600 thus its relative contribution decreased with height, especially in haze aggravating  
 601 processes (Fig.8). Although the contribution of the NO+OH reaction to daytime  
 602 HONO was small near the surface, its relative contribution to HONO increased with  
 603 height, especially in clean days (Fig.8). As for Phot<sub>nitrate</sub>, a much larger enhancement

Deleted: was  
 Deleted: in the first model layer

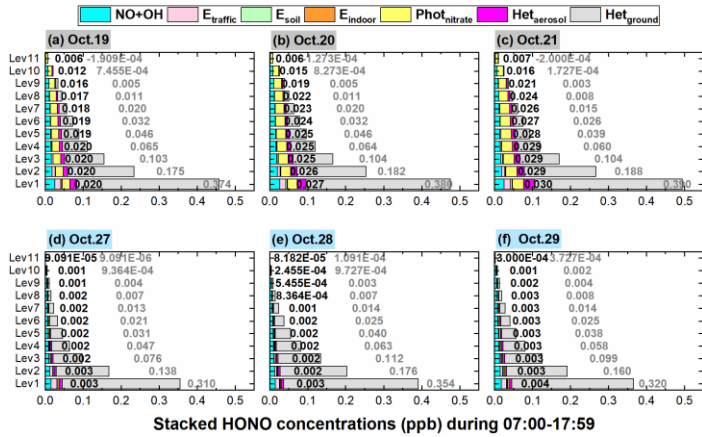
608 could be found in hazy days compared with clean days. In clean days the daytime  
609 enhanced HONO by  $\text{Phot}_{\text{nitrate}}$  was only 1–3 ppt in general and its contribution to  
610 daytime HONO was usually <10%, while in the haze aggravating process, the  
611 enhanced HONO concentration by  $\text{Phot}_{\text{nitrate}}$  was about ten times higher than that in  
612 clean days and  $\text{Phot}_{\text{nitrate}}$  became the dominant HONO source (~30–70%) at higher  
613 altitude, and both HONO concentrations and contributions by  $\text{Phot}_{\text{nitrate}}$  increased with  
614 the air pollution aggravation (**Fig.7a–c**, **Fig.8a–c**). The contributions of direct  
615 emission sources were small and decreased when  $\text{PM}_{2.5}$  increased, compared with  
616 those heterogeneous reactions. Higher concentrations of  $\text{NO}_2$ , nitrate, and  $\text{PM}_{2.5}$   
617 favored heterogeneous formation of HONO, while direct emission sources were  
618 relatively invariable under different pollution levels.

619 Based on our results, nitrate concentrations increased with the haze aggravating  
620 processes (**Fig.2b**), as a positive feedback effect, the elevated nitrate could in turn  
621 enhance HONO formation and further enhance the atmospheric oxidation capacity  
622 during daytime. Considering  $J_{\text{nitrate}}$  was still unclear, sensitivity tests were conducted  
623 and are presented in the discussion section.

624

Deleted: one order of magnitude

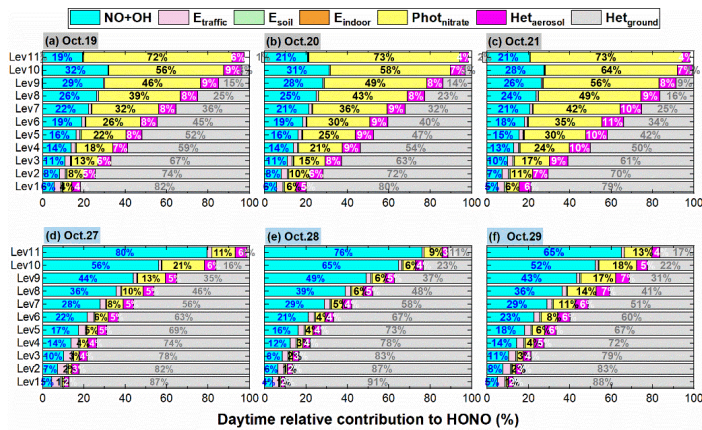
Deleted:  $\text{Phot}_{\text{nitrate}}$



Stacked HONO concentrations (ppb) during 07:00-17:59

627  
 628 **Figure 7** The 95-NCP-site-averaged daytime HONO concentrations at different heights when the  
 629 NO+OH reaction and the six potential HONO sources were included during a typical haze  
 630 aggravating process of Oct.19–21 (a–c) and a clean period of Oct.27–29 (d–f) of 2018. (The first  
 631 column numbers in black in each graph are for Phot<sub>nitrate</sub>, and the second column numbers in gray  
 632 are for Het<sub>ground</sub>).

Deleted: .



Daytime relative contribution to HONO (%)

634  
 635 **Figure 8** The 95-NCP-site-averaged relative contributions of the NO+OH reaction and each of the  
 636 six potential HONO sources to daytime HONO concentrations at different heights during a typical

638 haze aggravating process of Oct.19–21 (a–c) and a clean period of Oct.27–29 (d–f) of 2018. (The  
639 first column numbers in blue in each graph are for the NO+OH reaction, the second column  
640 numbers in black are for  $\text{Phot}_{\text{nitrate}}$ , the third column numbers in white are for  $\text{Het}_{\text{aerosol}}$ , and the  
641 fourth column numbers in gray are for  $\text{Het}_{\text{ground}}$ ).

Deleted: .

### 643 3.3.2 Enhanced OH and its production rate

644 **Fig.9** demonstrates daytime variations of OH production (P(OH)) and loss  
645 (L(OH)) rates near the surface and in the vertically-averaged layer (from ground to  
646 the height of 2.5km) at the 95 NCP sites for the Base and 6S cases during Oct.11–31,  
647 2018. A significant enhancement of P/L(OH) can be found near the surface and  
648 vertically, the six potential HONO sources accelerated OH production and loss rates  
649 remarkably near the surface and noticeably in the considered vertical layers.

Deleted: S

Deleted: could

Moved (insertion) [1]

Deleted: In short

650 Near the surface, daytime P(OH) and L(OH) were significantly enhanced by ~320%  
651 for the 6S case (mean was  $5.27 \text{ ppb h}^{-1}$ ) compared with the base case (mean was  $1.26$   
652  $\text{ ppb h}^{-1}$ ). For the base case, the daytime P(OH) via the photolysis of HONO and  $\text{O}_3$   
653 was  $0.09 \text{ ppb h}^{-1}$  and  $0.09 \text{ ppb h}^{-1}$ , respectively, while the daytime L(OH) via the  
654 NO+OH reaction was  $0.11 \text{ ppb h}^{-1}$  and the net contribution of HONO photolysis to  
655 P(OH) was  $-0.02 \text{ ppb h}^{-1}$ . After adding the six potential HONO sources in case 6S, the  
656 daytime P(OH) via the photolysis of HONO and  $\text{O}_3$  was  $1.81 \text{ ppb h}^{-1}$  and  $0.10 \text{ ppb h}^{-1}$ ,  
657 respectively, the daytime L(OH) via the NO+OH reaction was  $0.48 \text{ ppb h}^{-1}$  and the net  
658 contribution of HONO photolysis to P(OH) reached  $1.33 \text{ ppb h}^{-1}$ . HONO photolysis

Deleted: the

Deleted: photolysis

Deleted: photolysis

Deleted: .

Formatted: Superscript

Formatted: Superscript

667 was the main source of the primary formation of OH, while the secondary formed OH  
 668 via [the reaction of HO<sub>2</sub>+NO](#) (3.14 ppb h<sup>-1</sup>) was the dominant source of the total OH  
 669 formation.

670 Vertically, daytime P(OH) or L(OH) was enhanced by ~105% for the 6S case  
 671 (mean was 2.21 ppb h<sup>-1</sup>) compared with the base case (mean was 1.08 ppb h<sup>-1</sup>). [For](#)  
 672 [the base case, the daytime P\(OH\) via the photolysis of HONO and O<sub>3</sub> was 0.06 ppb](#)  
 673 [h<sup>-1</sup> and 0.10 ppb h<sup>-1</sup>, respectively, while the daytime L\(OH\) via the NO+OH reaction](#)  
 674 [was 0.07 ppb h<sup>-1</sup> and the net contribution of HONO photolysis to P\(OH\) was -0.01](#)  
 675 [ppb h<sup>-1</sup>. After coupling the six potential HONO sources in case 6S,](#) the daytime P(OH)  
 676 via the photolysis of HONO and O<sub>3</sub> and via the HO<sub>2</sub>+NO reaction was 0.48 ppb h<sup>-1</sup>,  
 677 0.12 ppb h<sup>-1</sup> and 1.52 ppb h<sup>-1</sup>, respectively, [the daytime L\(OH\) via the NO+OH](#)  
 678 [reaction was 0.15 ppb h<sup>-1</sup> and the net contribution of HONO photolysis to P\(OH\) was](#)  
 679 [0.33 ppb h<sup>-1</sup>.](#)

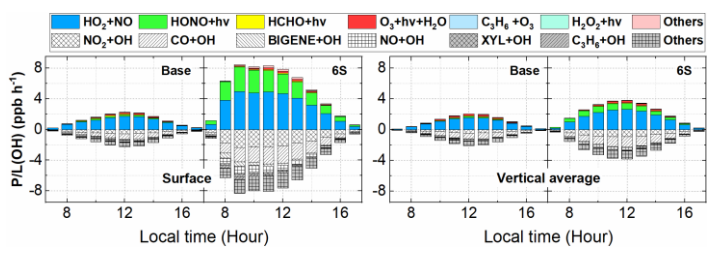
Deleted:

Deleted: ),

Deleted: the

Deleted: photolysis

Moved up [1]: In short, the six potential HONO sources accelerated OH production and loss rates remarkably near the surface and noticeably in the considered vertical layers.



681  
 682 **Figure 9** Diurnal mean variations of OH production (P(OH)) and loss (L(OH)) rates including  
 683 major production and loss reactions near the surface and in the vertically-averaged layer (from  
 684 ground to the height of 2.5km) at the 95 NCP sites for the Base and 6S cases during Oct.11–31,  
 685 2018.

693

694 **Fig.10** shows the linear relationships between daytime-averaged P(OH) and  
695 PM<sub>2.5</sub> concentrations and between daytime-averaged OH and PM<sub>2.5</sub> concentrations  
696 from ground to the height of 2.5km at the 95 NCP sites during Oct. 11–31 of 2018.

697 Both P(OH) for the two cases (Base and 6S) and the enhanced P(OH) due to the six  
698 potential HONO sources showed a strong positive correlation ( $r > 0.8$ ) with PM<sub>2.5</sub>

699 concentrations at the 95 NCP sites, because Het<sub>aerosol</sub>, Het<sub>ground</sub> and Phot<sub>nitrate</sub> were  
700 significantly increased with the elevated PM<sub>2.5</sub>. The enhanced P(OH) for the 6S case

701 reached 0.043 ppb h<sup>-1</sup> per 1 μg m<sup>-3</sup> of a PM<sub>2.5</sub> enhancement. Similarly, high positive  
702 correlation ( $r > 0.6$ ) could be found between OH and PM<sub>2.5</sub> concentrations, the OH

703 concentrations and enhancements due to the six potential HONO sources were both  
704 higher in hazy days than those in clean days, and the enhancement of OH reached  
705  $3.62 \times 10^4$  molec cm<sup>-3</sup> per μg m<sup>-3</sup> of PM<sub>2.5</sub> for case 6S. These results were consistent

706 with a recent field study reported by Slater et al. (2020), who found that the OH  
707 observed in haze events was elevated in central Beijing in November–December of  
708 2016. Furthermore, two observations confirmed the key role of HONO in producing

709 primary OH despite the relatively lower photolysis frequency in haze aggravating  
710 processes (Slater et al., 2020; Tan et al., 2018), consistent with our simulations

711 (**Fig.S7** shows the relationship between surface PM<sub>2.5</sub> and photolysis frequencies of  
712 NO<sub>2</sub>, HONO and HNO<sub>3</sub> in this study).

Deleted: R

Formatted: Subscript

Formatted: Subscript

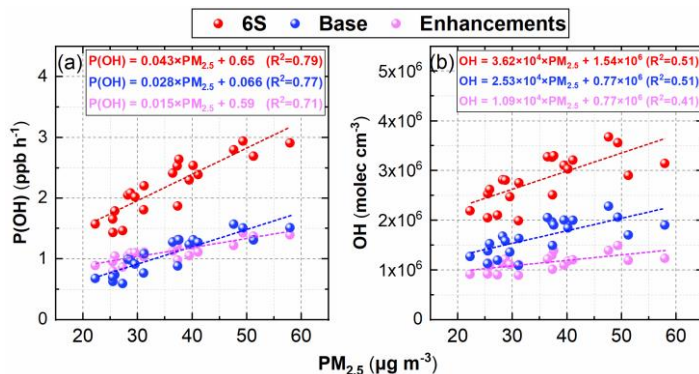
Deleted: , which are related to PM<sub>2.5</sub> concentrations and solar radiation, are dominant potential HONO sources...

Deleted: and the

Formatted: Subscript

Deleted: R

Deleted: S6

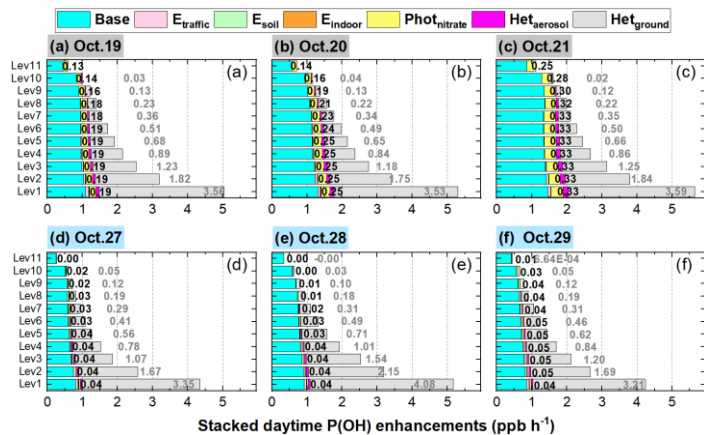


719  
 720 **Figure 10** The linear relationships between daytime-averaged P(OH) and PM<sub>2.5</sub> concentrations (a)  
 721 and between daytime-averaged OH and PM<sub>2.5</sub> concentrations (b) from ground to the height of  
 722 2.5km at the 95 NCP sites during Oct. 11–31 of 2018.

723  
 724 **Figs.11&12** show the detailed comparisons of P(OH) and OH enhancements  
 725 during a haze aggravating process and a clean period. It can be seen that both P(OH)  
 726 and OH were enhanced in hazy days compared with clean days, and P(OH) and OH  
 727 increased with the aggravated haze pollution. Among the six potential HONO sources,  
 728 Het<sub>ground</sub> was the largest contributor to the enhanced P(OH) and OH near the surface,  
 729 but its contribution was relatively stable under different pollution levels and was  
 730 attenuated rapidly with height in both hazy and clean days; the contribution induced  
 731 by Phot<sub>nitrate</sub> was remarkably increased in haze aggravating processes and was about  
 732 ten times higher than that in clean days; Het<sub>aerosol</sub> also increased with the pollution  
 733 levels but with relatively small values, while the impact of other three direct emission  
 734 sources of HONO was quite small.

Deleted: one order of magnitude

735

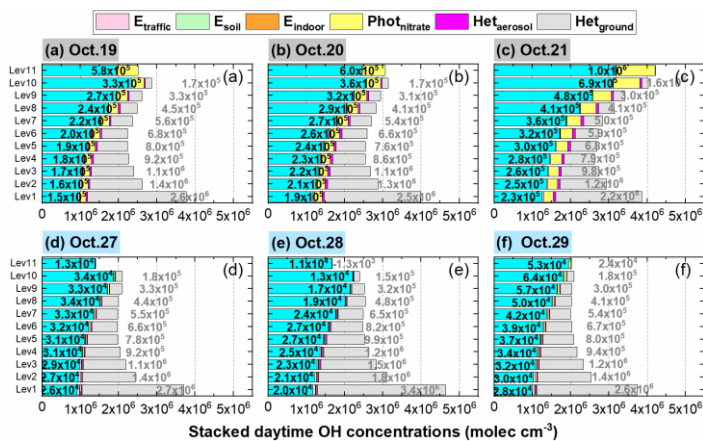


737

738 **Figure 11** The 95-NCP-site-averaged daytime P(OH) for the base case and the enhancements due to  
 739 the six potential HONO sources during a typical haze aggravating process of Oct.19–21 (a–c)  
 740 and a clean period of Oct.27–29 (d–f) of 2018. (The first column number in black in each graph is  
 741 for Phot<sub>nitrate</sub>, and the second column number in gray is for Het<sub>ground</sub>).

742

Deleted: .



743

744 **Figure 12** The 95-NCP-site-averaged daytime OH concentrations for the base case and the  
 745 enhancements due to the six potential HONO sources during a typical haze aggravating process of  
 746 Oct.19–21 (a–c) and a clean period of Oct.27–29 (d–f) of 2018. (The first column number in black  
 747 is for Phot<sub>nitrate</sub>, and the second column number in gray is for Het<sub>ground</sub>).

Deleted: .



749 in each graph is for  $Phot_{nitrate}$ , and the second column number in gray is for  $Het_{ground}$ ).

750

751 **3.3.3 Enhanced DMA8 O<sub>3</sub>**

Deleted: 2

752 **Fig.13** demonstrates the linear relationship between DMA8 O<sub>3</sub> enhancements and

753 daytime PM<sub>2.5</sub> concentrations in each vertical layer and the averaged vertical layer for

Deleted: (a)

754 the considered eleven layers at the 95 NCP sites during Oct. 11–31 of 2018. A good

Deleted: (b)

755 correlation ( $r > 0.8$ ) between DMA8 O<sub>3</sub> enhancements and daytime PM<sub>2.5</sub>

Deleted:

756 concentrations in the vertical averaged layer ([similar reasons for the strong positive](#)

Deleted: R

757 [correlation between the enhanced P\(OH\) and PM<sub>2.5</sub> concentrations shown above](#))

758 suggests that the enhanced O<sub>3</sub> due to the six potential HONO sources was larger in

759 polluted days and increased during the haze aggravating processes. The enhanced

760 DMA8 O<sub>3</sub> was < 2ppb when PM<sub>2.5</sub> was < 20 $\mu\text{g m}^{-3}$  and was >10 ppb when PM<sub>2.5</sub> was >

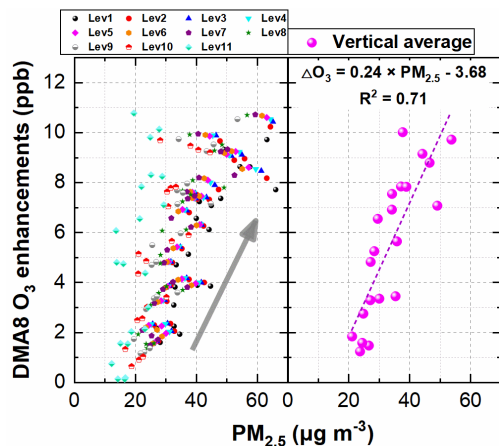
Deleted: ,

761 60 $\mu\text{g m}^{-3}$  on average, with a mean DMA8 O<sub>3</sub> enhancement of 0.24 ppb per  $\mu\text{g m}^{-3}$  of

Deleted: u

762 PM<sub>2.5</sub>.

763



771

772 **Figure 13** The linear relationship between DMA8 O<sub>3</sub> enhancements and daytime PM<sub>2.5</sub>  
 773 concentrations in each vertical layer (a) and the averaged vertical layer for the considered eleven  
 774 layers (b) at the 95 NCP sites during Oct. 11–31 of 2018.

775

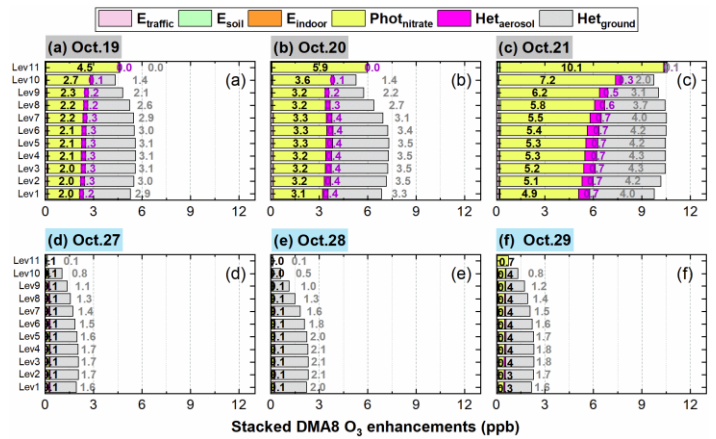
776 **Fig.14** shows the 95-NCP-site-averaged DMA8 O<sub>3</sub> enhancements due to the six  
 777 potential HONO sources during a typical haze aggravating process of Oct.19–21 and  
 778 a clean period of Oct.27–29 of 2018. A significant enhancement of DMA8 O<sub>3</sub> can be  
 779 found during the haze aggravating process compared with during clean days. The  
 780 enhanced DMA8 O<sub>3</sub> was ~5.5 ppb (Oct.19), ~ 7 ppb (Oct.20) and ~ 10 ppb (Oct.21),  
 781 respectively, during the haze aggravating process, while that was usually ~2 ppb in  
 782 clean days.

783 In clean days, Het<sub>ground</sub> was the dominant contributor (~1.5–2 ppb) to the  
 784 enhanced DMA8 O<sub>3</sub> among the six potential HONO sources, the contribution of  
 785 Phot<sub>nitrate</sub> to the enhanced DMA8 O<sub>3</sub> was ~0.1–0.4 ppb, while that of the other four  
 786 sources was minor. When it comes to the comparison between the haze aggravating

787 process (Oct.19–21) and clean days, the DMA8 O<sub>3</sub> enhancements induced by Het<sub>ground</sub>  
 788 were doubled and reached ~3–4 ppb; the contribution of Phot<sub>nitrate</sub> to the enhanced  
 789 DMA8 O<sub>3</sub> substantially increased and reached ~2–4.5 ppb (Oct.19), ~3–6 ppb (Oct.20)  
 790 and ~5–10 ppb (Oct.21), respectively; Het<sub>aerosol</sub> showed an increasing contribution to  
 791 the enhanced DMA8 O<sub>3</sub> during haze aggravating process (~0.3 ppb on Oct.19, ~0.4  
 792 ppb on Oct.20 and ~0.7 ppb on Oct.21), while the impacts of the other three direct  
 793 emission sources (E<sub>traffic</sub>, E<sub>soil</sub>, and E<sub>indoor</sub>) on the enhanced DMA8 O<sub>3</sub> were minor.

Deleted: in  
 Deleted: in  
 Deleted: in

794



795

796 **Figure 14** The 95-NCP-site-averaged DMA8 O<sub>3</sub> enhancements due to the six potential HONO  
 797 sources during a typical haze aggravating process of Oct.19–21 (a–c) and a clean period of  
 798 Oct.27–29 (d–f) of 2018. (The column in black numbers in each graph is for Phot<sub>nitrate</sub>, the column  
 799 in purple numbers in each graph is for Het<sub>aerosol</sub>, and the column in gray numbers is for Het<sub>ground</sub>).

Deleted: .

800

### 805 3.4 Vertical variations of O<sub>3</sub>-NO<sub>x</sub>-VOCs sensitivity

806 Based on the results above, Phot<sub>nitrate</sub> could significantly enhance the DMA8 O<sub>3</sub>  
807 by ten times in the considered vertical layers (especially at elevated heights) in  
808 polluted events, but previous studies have not fully discussed. To better understand its  
809 role in vertical O<sub>3</sub> formation, the O<sub>3</sub>-NO<sub>x</sub>-VOCs sensitivity was analyzed by using the  
810 P(H<sub>2</sub>O<sub>2</sub>)/P(HNO<sub>3</sub>) ratio proposed by Sillman (1995), which is more suitable than the  
811 concentration ratio of H<sub>2</sub>O<sub>2</sub>/HNO<sub>3</sub> because of the large dry deposition velocity of the  
812 two gases in the troposphere (Sillman, 1995). A transition point of P(H<sub>2</sub>O<sub>2</sub>)/P(HNO<sub>3</sub>)  
813 = 0.35 was suggested by Sillman (1995), when P(H<sub>2</sub>O<sub>2</sub>)/P(HNO<sub>3</sub>) was <0.35, O<sub>3</sub>  
814 shows VOCs-sensitive chemistry (increasing VOC concentrations can significantly  
815 elevate O<sub>3</sub> levels) and when P(H<sub>2</sub>O<sub>2</sub>)/P(HNO<sub>3</sub>) was >0.35, O<sub>3</sub> tends to NO<sub>x</sub>-sensitive  
816 chemistry (increasing NO<sub>x</sub> concentrations can significantly elevate O<sub>3</sub> levels).

817 **Fig.15** demonstrates the 95-NCP-site-averaged P(H<sub>2</sub>O<sub>2</sub>)/P(HNO<sub>3</sub>) ratio at each  
818 vertical layer for the 6S case during a typical haze aggravating process of Oct.19–21  
819 and a clean period of Oct.27–29 of 2018. Obviously opposite O<sub>3</sub> sensitivity appeared  
820 between the lower layers (VOCs sensitive) and the higher layers (NO<sub>x</sub> sensitive) in  
821 both clean and hazy days, and the transition point usually appeared at the eighth layer  
822 (~600–800 m).

823 The Phot<sub>nitrate</sub> reaction is assumed to produce HONO and NO<sub>x</sub> (Zhou et al., 2003;  
824 Romer et al., 2018; Gen et al., 2022), this reaction not only enhances OH  
825 concentrations via HONO photolysis, but also directly releases NO<sub>x</sub> back into the  
826 troposphere. Considering the NO<sub>x</sub>-sensitive O<sub>3</sub> chemistry at higher layers (>800m),

Deleted: one order of magnitude

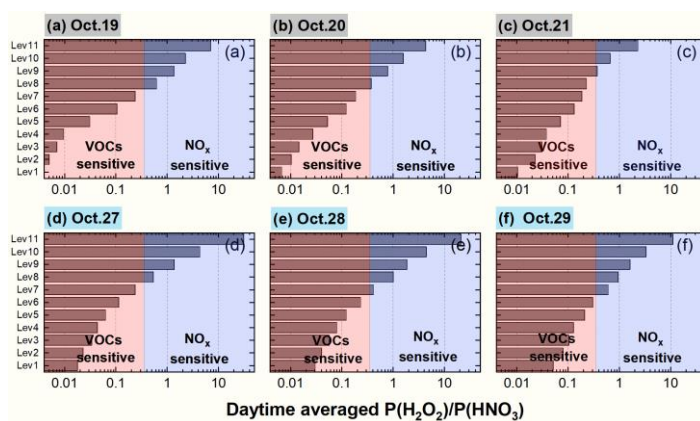
Deleted: nitrate photolysis

Formatted: Subscript

829 elevating OH and NO<sub>x</sub> concentrations are both favorable for O<sub>3</sub> formation, especially  
 830 in haze aggravating processes with abundant nitrate (detailed vertically enhanced O<sub>3</sub>  
 831 production/loss rates induced by Phot<sub>nitrate</sub> are [shown in Fig.S8](#)).

Deleted: given

Deleted: 7



833  
 834 **Figure 15** The 95-NCP-site-averaged P(H<sub>2</sub>O<sub>2</sub>)/P(HNO<sub>3</sub>) ratio at each vertical layer for the 6S case  
 835 during a typical haze aggravating process of Oct.19–21 (a–c) and a clean period of Oct.27–29 (d–f)  
 836 of 2018.

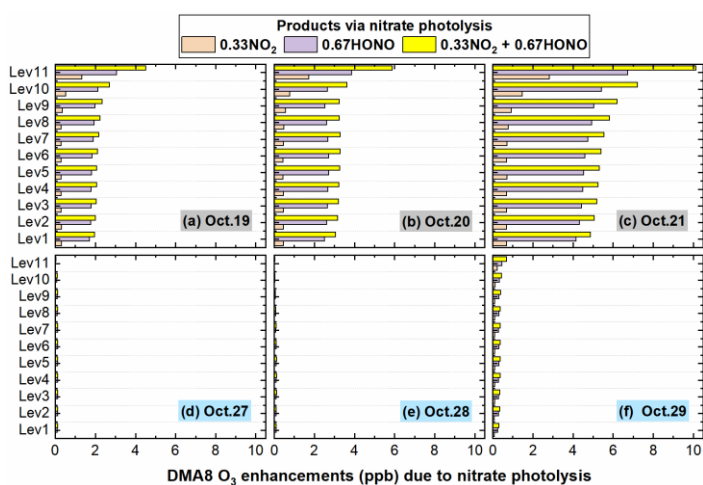
837  
 838 The specific role of the produced HONO or NO<sub>2</sub> via the [Phot<sub>nitrate</sub>](#) reaction (R2) in  
 839 DMA8 O<sub>3</sub> enhancements [was](#) further analyzed and is shown in **Fig. 16**, the produced  
 840 NO<sub>2</sub> and HONO jointly promoted O<sub>3</sub> formation and increased DMA8 O<sub>3</sub>  
 841 concentrations. From the surface to ~1200m (Level 9), the DMA8 O<sub>3</sub> enhancements  
 842 for case D\_HONO was ~5 times those for case D\_NO<sub>2</sub>, while at ~2000 m (Level 11)  
 843 the DMA8 O<sub>3</sub> enhancements for case D\_HONO was ~2 times those for case D\_NO<sub>2</sub>.  
 844 A balance exists between the propagation of the free radical interconversion cycle and  
 845 the rate of termination of the cycle for the O<sub>3</sub> formation chemistry (Gligorovski et al.,

Deleted: nitrate photolysis

Formatted: Subscript

Deleted: were

850 2015), considering the 0.67 and 0.33 yields (ratio is 2) for the two products, we could  
 851 conclude that the impact of produced HONO on O<sub>3</sub> enhancements was larger than [that](#)  
 852 [of](#) produced NO<sub>2</sub> near the surface, while at higher altitude (>2000 m) the impacts of  
 853 the two products were similar.  
 854



855  
 856 **Figure 16** The 95-NCP-site-averaged DMA8 O<sub>3</sub> enhancements due to nitrate photolysis with three  
 857 product scenarios (cases D\_NO<sub>2</sub>, D\_HONO and D) during a typical haze aggravating process of  
 858 Oct.19–21 (a–c) and a clean period of Oct.27–29 (d–f) in 2018.

859  
 860 **4. Discussion**

861 **4.1 Vertical variations of potential HONO sources**

862 The relative contribution of potential HONO sources near the surface,  
 863 corresponding to the first model layer (0 to ~35 m) in our simulation, was quantified

864 in previous modelling studies (Fu et al., 2019; Xue et al., 2020; Zhang et al., 2021),  
865 however, for those potential HONO sources, their relative contributions to HONO  
866 concentrations near and above the surface should be different. Based on our results  
867 **(Figs.7&8)**, the effects of aerosol related HONO sources would be severely  
868 underestimated in hazy days when only focused surface HONO, especially for  
869 [Phot<sub>nitrate</sub>](#). Near the surface in NCP, the daytime contribution of Phot<sub>nitrate</sub> to HONO  
870 concentrations in hazy days was only ~4–6%, but this source contributed ~35–50% of  
871 the enhanced DMA8 O<sub>3</sub> **(Fig.14a–c)**; above the eighth layer (~800 m), this source  
872 contributed ~50–70% of HONO concentrations and ~50–95% of the enhanced DMA8  
873 O<sub>3</sub> **(Fig.14a–c)**.

874 A recent observation in urban Beijing reported vertical HONO concentrations  
875 from three heights above the [ground](#) and found that extremely high HONO  
876 concentrations occurred at 120 m (~5 ppb) and 240 m (~3 ppb) rather than near the  
877 surface (~1.2 ppb) during 12:00 in a typical hazy day (Zhang et al., 2020b). The  
878 observation was unusual at noontime under strong convection conditions, inconsistent  
879 with those most previous observations indicating a HONO decrease trend with height,  
880 especially with the observational results of Zhu et al. (2011) and Meng et al. (2020)  
881 and simulated results of Zhang et al. (2021) **and ours in Fig.S6** at the same  
882 observational site. The contributions of different HONO sources at each layer were  
883 analyzed by using a box model, but ~80–90% of the noontime HONO at higher layers  
884 could not be explained by the known HONO formation mechanisms (Zhang et al.,  
885 2019c). The box model neglected the vertical convection, so the ground related

Formatted: Font: Bold

Deleted: nitrate photolysis

Formatted: Subscript

Deleted: surface

Formatted: Font: Bold

Deleted: (including our simulations in Fig.S5)

889 HONO sources had no contribution to HONO concentrations at the higher layers, thus  
890 their HONO simulations were actually underestimated compared with our results and  
891 the previous studies of Wong et al. (2011) and Zhang et al. (2021).

892

## 893 4.2 Uncertainties of $J_{\text{nitrate}}/J_{\text{HNO}_3}$ ratios and their impacts

### 894 4.2.1 Uncertainties of $J_{\text{nitrate}}/J_{\text{HNO}_3}$ ratios in DMA8 O<sub>3</sub> enhancements

895 Based on our results,  $H_{\text{etground}}$  and  $Ph_{\text{otnitrate}}$  were the two major contributors to  
896 the enhanced DMA8 O<sub>3</sub>, especially for  $Ph_{\text{otnitrate}}$  in hazy days with higher PM<sub>2.5</sub>  
897 concentrations. The uncertainties of  $Ph_{\text{otnitrate}}$  (four  $J_{\text{nitrate}}/J_{\text{HNO}_3}$  ratios) in O<sub>3</sub>  
898 enhancements were analyzed and are shown in Fig.17 (The uncertainties of  $H_{\text{etground}}$   
899 are presented in text S2). During the haze aggravating process, the enhanced DMA8  
900 O<sub>3</sub> near the surface increased from ~0.3 to ~0.5 ppb, from ~0.9 to ~2 ppb, from ~2 to  
901 ~6 ppb, and from ~5 to ~12 ppb, with the  $J_{\text{nitrate}}/J_{\text{HNO}_3}$  ratio being 1, 7, 30, 120,  
902 respectively, and the enhanced O<sub>3</sub> increased with altitude. In clean days, the impact of  
903  $Ph_{\text{otnitrate}}$  on O<sub>3</sub> enhancements was small (<1 ppb) even with a  $J_{\text{nitrate}}/J_{\text{HNO}_3}$  ratio of  
904 120.

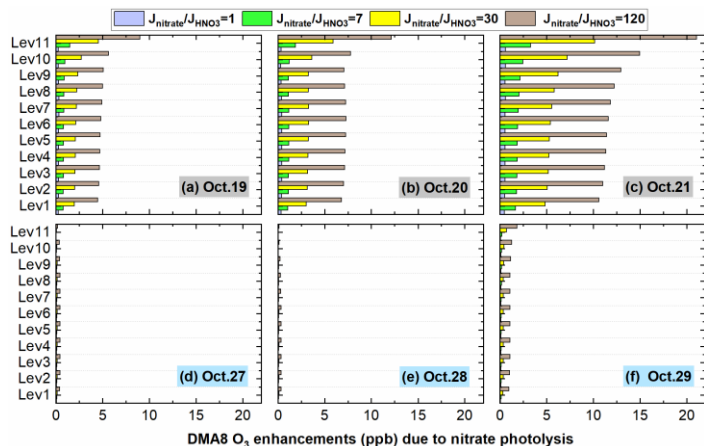
905

Deleted: the

Deleted: for

Deleted: given





909

910 **Figure 17** The 95-NCP-site-averaged DMA8 O<sub>3</sub> enhancement induced by nitrate photolysis with  
 911 four J<sub>nitrate</sub>/J<sub>HNO<sub>3</sub></sub> ratios (1, 7, 30 and 120) during a typical haze aggravating process of Oct.19–21  
 912 (a–c) and a clean period of Oct.27–29 (d–f) of 2018.

913

#### 914 4.2.2 Uncertainties of J<sub>nitrate</sub>/J<sub>HNO<sub>3</sub></sub> ratios in nitrate concentrations

915 We found considerable enhancements in O<sub>3</sub> concentrations induced by Phot<sub>nitrate</sub>,  
 916 yet it is still unclear that to what extent Phot<sub>nitrate</sub> could influence nitrate  
 917 concentrations. The overall nitrate concentrations for the base case and the nitrate  
 918 enhancements induced by the potential HONO sources decreased with rising altitude  
 919 except for Phot<sub>nitrate</sub> (Fig.S9a). Het<sub>ground</sub> enhanced nitrate concentrations by ~1.5 μg  
 920 m<sup>-3</sup> near the surface and the enhancements decreased to < 0.5 μg m<sup>-3</sup> above the eighth  
 921 model layer (~800m); the nitrate enhancements due to Het<sub>aerosol</sub> and E<sub>traffic</sub> near the  
 922 surface were ~0.2 and ~0.1 μg m<sup>-3</sup>, respectively, and were < 0.1 and < 0.04 μg m<sup>-3</sup>  
 923 above the sixth model layer (~500m). For Phot<sub>nitrate</sub>, the overall impact of four

Deleted: nitrate photolysis

Formatted: Subscript

Deleted: nitrate photolysis

Formatted: Subscript

Deleted: S8a

927  $J_{\text{nitrate}}/J_{\text{HNO}_3}$  ratios on nitrate concentrations is shown in **Fig.S9b**, a smaller  $J_{\text{nitrate}}/J_{\text{HNO}_3}$   
928 ratio of 1 or 7 had a limited impact on nitrate concentrations of  $\sim 0\text{--}0.05 \mu\text{g m}^{-3}$ , a  
929  $J_{\text{nitrate}}/J_{\text{HNO}_3}$  ratio of 30 slightly decreased nitrate concentrations by  $\sim 0.2 \mu\text{g m}^{-3}$ , while  
930 the  $J_{\text{nitrate}}/J_{\text{HNO}_3}$  ratio of 120 decreased vertical nitrate concentrations by  $\sim 0.3\text{--}0.8 \mu\text{g}$   
931  $\text{m}^{-3}$ . The relative nitrate changes caused by  $\text{Phot}_{\text{nitrate}}$  were calculated by the  
932 differences between four cases added  $\text{Phot}_{\text{nitrate}}$  (cases Nit\_1, Nit\_7, D and Nit\_120)  
933 and the base case (**Fig.S9c**). The vertical nitrate concentrations were reduced by  $\sim 0\text{--}$   
934  $0.4\%$  ( $J_{\text{nitrate}}/J_{\text{HNO}_3}=1$ ),  $\sim 0\text{--}2\%$  (7),  $\sim 2\text{--}5\%$  (30) and  $\sim 10\text{--}14\%$  (120) at the 95 NCP  
935 sites, meaning that the  $\text{Phot}_{\text{nitrate}}$  impact on vertical nitrate concentrations is limited  
936 ( $<5\%$ ) when adopting a relatively small  $J_{\text{nitrate}}/J_{\text{HNO}_3}$  ratio ( $< 30$ ) (**Fig.S9c**).

937 **Romer et al. (2018) found a  $J_{\text{nitrate}}/J_{\text{HNO}_3}$  ratio of 10 or 30 had a much larger effect**  
938 **on HONO than on  $\text{HNO}_3$ , and  $\text{Phot}_{\text{nitrate}}$  accounted for an average of 40% of the total**  
939 **production of HONO, and only 10% of  $\text{HNO}_3$  loss with a  $J_{\text{nitrate}}/J_{\text{HNO}_3}$  ratio of 10**  
940 **(Fig.5 in Romer et al. (2018)), consistent with our study. From the production rate of**  
941 **gas  $\text{HNO}_3$  ( $P_{\text{HNO}_3}$ ) in Fig.S10, we can find that an increase in the  $J_{\text{nitrate}}/J_{\text{HNO}_3}$  ratio for**  
942  **$\text{Phot}_{\text{nitrate}}$  simultaneously enhances the  $\text{HNO}_3$  production rate, and is favorable for**  
943 **nitrate formation via the reaction between  $\text{HNO}_3$  and  $\text{NH}_3$ . Nitrate consumption is**  
944 **mitigated by the faster nitrate formation, this is the main reason for less perturbation**  
945 **of the nitrate budget influenced by  $\text{Phot}_{\text{nitrate}}$ .**

946 **Fig.18** shows the detailed relative changes of nitrate caused by  $\text{Phot}_{\text{nitrate}}$  during a  
947 typical haze aggravating process and a clean period (corresponding concentrations are  
948 shown in **Fig.S11**). The percentage nitrate reduction was usually smaller in hazy days

Deleted: S8b

Deleted: ,

Deleted: the

Deleted: S8c

Formatted: Subscript

Formatted: Subscript

Formatted: Subscript

Formatted: Subscript

Deleted: HONO

Deleted: but

Formatted: Subscript

Formatted: Subscript

Formatted: Subscript

Deleted: which is

Deleted: gaseous  $\text{HNO}_3$

Formatted: Subscript

Formatted: Subscript

Formatted: Font: Bold

Deleted: could

Deleted: increasing

Formatted: Subscript

Formatted: Subscript

Formatted: Subscript

Deleted: cing

Formatted: Subscript

Deleted: which

Formatted: Subscript

Formatted: Subscript

Deleted: was

Deleted: why

Formatted: Subscript

Deleted: nitrate

Deleted: were

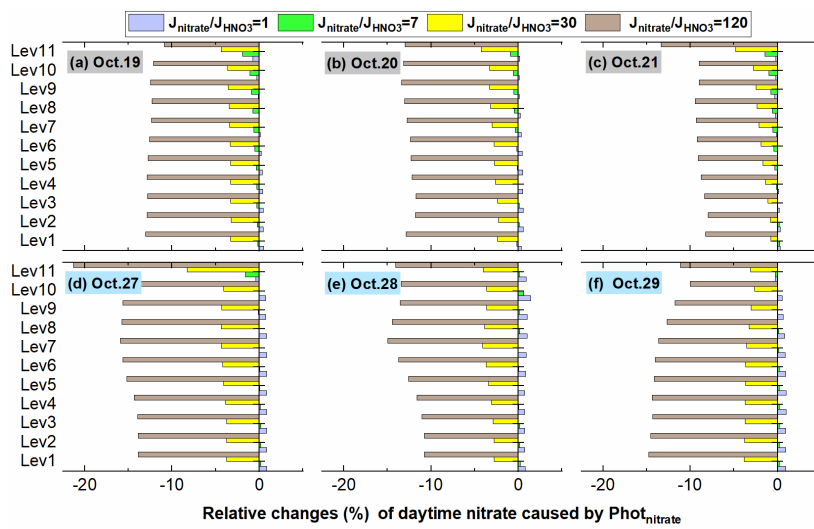
Deleted: S9

Deleted: ),

Deleted: the

968 than in clean days, mainly due to the slightly weaker photolysis frequency in pollution  
 969 events (Fig.S7). The nitrate reduction was <5% when adopting a  $J_{\text{nitrate}}/J_{\text{HNO}_3}$  ratio of  
 970 30 in both clean and hazy days and was <15% in most cases even when the  
 971  $J_{\text{nitrate}}/J_{\text{HNO}_3}$  ratio reached 120.

972



973

974 **Figure 18** The 95-NCP-site-averaged relative changes of nitrate with four  $J_{\text{nitrate}}/J_{\text{HNO}_3}$  ratios (1, 7,  
 975 30 and 120) compared with the base case, during a typical haze aggravating process of Oct.19–21  
 976 (a–c) and a clean period of Oct.27–29 (d–f) of 2018.

977

### 978 4.2.3 Possible ranges of the $J_{\text{nitrate}}/J_{\text{HNO}_3}$ ratio

979 From the above discussion, we can find that the enhanced OH and O<sub>3</sub> due to  
 980  $\text{Phot}_{\text{nitrate}}$  are remarkable during haze aggravating processes, and the exact value of the  
 981  $J_{\text{nitrate}}/J_{\text{HNO}_3}$  ratio requires more studies.

- Formatted: Font: Bold
- Deleted: and nitrate was slightly reduced during the haze aggravating processes, t...
- Deleted: the
- Deleted: in
- Deleted: days
- Deleted: of the
- Deleted: .

- Deleted: nitrate
- Deleted: (c)

991 **Fig. 19** shows diurnal patterns of surface-averaged and vertically-averaged  
992 simulations of the  $J_{\text{Phot}_{\text{nitrate}}}$  frequency with four different  $J_{\text{nitrate}}/J_{\text{HNO}_3}$  ratios at the 95  
993 NCP sites during the study period. The  $J_{\text{Phot}_{\text{nitrate}}}$  frequency at 12:00 was  $3.7 \times 10^{-7}$ ,  
994  $2.6 \times 10^{-6}$ ,  $1.1 \times 10^{-5}$  and  $4.5 \times 10^{-5} \text{ s}^{-1}$ , when adopting a  $J_{\text{nitrate}}/J_{\text{HNO}_3}$  ratio of 1, 7, 30 and  
995 120, respectively. The corresponding vertically-averaged  $J_{\text{Phot}_{\text{nitrate}}}$  frequency was  
996 slightly larger ( $\sim 10\%$ ) and was  $4.2 \times 10^{-7}$ ,  $2.9 \times 10^{-6}$ ,  $1.3 \times 10^{-5}$  and  $5.0 \times 10^{-5} \text{ s}^{-1}$ ,  
997 respectively. Adopting a  $J_{\text{nitrate}}/J_{\text{HNO}_3}$  ratio of 30 in the 6S case, with the corresponding  
998  $J_{\text{nitrate}}$  of  $1.1\text{--}1.3 \times 10^{-5} \text{ s}^{-1}$ , produced  $\sim 30\text{--}50\%$  of the enhanced  $\text{O}_3$  near the surface in  
999 hazy days (**Fig.13**), and  $\sim 70\text{--}90\%$  of the enhanced  $\text{O}_3$  at higher layers ( $>800 \text{ m}$ ).

1000 The reported values of  $J_{\text{nitrate}}$  from previous studies are summarized in **Table 4**.  
1001 The experimental  $J_{\text{nitrate}}$  values have been controversial over the past two decades and  
1002 are still arguable currently. In our simulations for the 6S case,  $J_{\text{Phot}_{\text{nitrate}}}$  contributed  
1003 from  $\sim 1\%$  (clean days) to  $\sim 5\%$  (hazy days) to surface HONO during daytime when  
1004 using the  $J_{\text{nitrate}}/J_{\text{HNO}_3}$  ratio of 30 in NCP, consistent with  $<8\%$  at a rural site in NCP  
1005 reported by Xue et al. (2020) and  $\sim 1\%$  at urban Beijing reported by Zhang et al. (2021)  
1006 using the same ratio; however, the increasing contribution of  $J_{\text{Phot}_{\text{nitrate}}}$  to HONO  
1007 concentrations with rising altitude based on our simulations (**Fig.7**), has not been  
1008 discussed in previous research. Furthermore, we found that the overall  $J_{\text{Phot}_{\text{nitrate}}}$   
1009 impact to OH and  $\text{O}_3$  would be severely underestimated when the  $J_{\text{Phot}_{\text{nitrate}}}$   
1010 contribution to vertical HONO was excluded.

1011 A larger  $J_{\text{nitrate}}/J_{\text{HNO}_3}$  ratio of 120 for  $J_{\text{Phot}_{\text{nitrate}}}$  ( $4.5\text{--}5.0 \times 10^{-5} \text{ s}^{-1}$  at 12:00) produced  
1012  $\sim 25\text{--}30\%$  of noontime HONO in NCP in our study (**Fig.S12**), comparable with  $30\text{--}40\%$

Deleted: nitrate photolysis

Formatted: Subscript

Deleted: nitrate photolysis

Formatted: Subscript

Deleted: nitrate photolysis

Formatted: Subscript

Deleted: nitrate photolysis

Formatted: Subscript

Deleted: nitrate photolysis

Formatted: Subscript

Formatted: Subscript

Deleted: of nitrate photolysis

Formatted: Subscript

Deleted: of nitrate photolysis

Deleted: nitrate photolysis

Formatted: Subscript

Deleted: S10

1022 in previous modelling studies (Fu et al., 2019; Shi et al., 2020) when using the  
1023  $J_{\text{nitrate}}/J_{\text{HNO}_3}$  ratio of 118.57 ( $8.3 \times 10^{-5}/ 7 \times 10^{-7}$ ). In haze aggravating processes, the  
1024 contribution of  $\text{Phot}_{\text{nitrate}}$  ( $J_{\text{nitrate}}/J_{\text{HNO}_3} = 120$ ) to the DMA8  $\text{O}_3$  enhancements reached  
1025  $\sim 5\text{--}10$  ppb near the surface and  $\sim 8\text{--}20$  ppb above the tenth model layer (Fig.17), these  
1026 enhancements were extremely large. In a previous modelling study by Fu et al. (2020),  
1027 the daytime surface  $\text{O}_3$  simulations were systematically overestimated by  $\sim 5$  ppb in  
1028 NCP in winter (Fig.S4 in Fu et al. (2020)), the inclusion of  $\text{Phot}_{\text{nitrate}}$  ( $J_{\text{nitrate}}/J_{\text{HNO}_3} =$   
1029 118.57) in their study might cause the overestimation. From the above, a  $J_{\text{nitrate}}/J_{\text{HNO}_3}$   
1030 ratio of 120, or a  $J_{\text{nitrate}}$  value of  $\sim 4\text{--}5 \times 10^{-5} \text{ s}^{-1}$  is possibly overestimated. When  
1031 adopting the maximum  $J_{\text{nitrate}}$  value of  $10^{-4} \text{ s}^{-1}$  reported by Ye et al. (2016a) and Bao et  
1032 al. (2018), we reasonably speculate that  $\text{O}_3$  simulations will be significantly  
1033 overestimated, especially at higher altitude with  $\text{NO}_x$ -sensitive  $\text{O}_3$  chemistry (Fig.15).

1034 Romer et al. (2018) and Kasibhatla et al. (2018) suggested that a  $J_{\text{nitrate}}/J_{\text{HNO}_3}$  ratio  
1035 of 30 or smaller would be more suitable, being about the minimum value reported by  
1036 Ye et al. (2016a) and Bao et al. (2018), this ratio has shown significant influence on  
1037 the  $\text{O}_3$  simulations in haze aggravating processes in this study. The lack of  
1038 photo-catalyzer in suspended submicron particulate sodium and ammonium nitrate  
1039 may cause a lower  $J_{\text{nitrate}}/J_{\text{HNO}_3}$  ratio ( $<10$ ) reported by Shi et al. (2021), so more  
1040 chamber experiments need to be conducted by using the particles collected in the real  
1041 atmosphere. Choosing a larger  $J_{\text{nitrate}}$  value might cover up other ground-based  
1042 unknown HONO sources, creating an illusion of good model simulations of daytime  
1043 HONO, but resulting in overestimation of  $\text{O}_3$  concentrations. Considering the

Deleted: s

Deleted: and

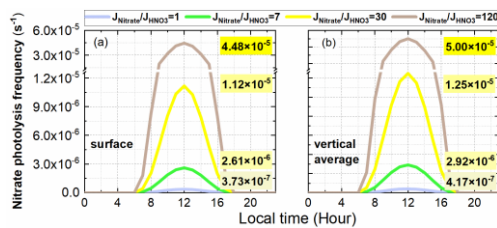
Deleted: ly

Deleted: d

Deleted: to

1049 uncertainties of NO<sub>x</sub> or VOCs emissions, which also significantly impact O<sub>3</sub>  
 1050 simulations, more studies are needed to find the exact value of J<sub>nitrate</sub> in the real  
 1051 atmosphere.

1052



1053

1054 **Figure 19** Diurnal patterns of surface-averaged (a) and vertically-averaged (b) simulations of the  
 1055 nitrate photolysis frequency with four different J<sub>nitrate</sub>/J<sub>HNO<sub>3</sub></sub> ratios (1, 7, 30, 120) at the 95 NCP  
 1056 sites during the study period (The nitrate photolysis frequencies at 12:00 are shown in each graph).

Deleted: is

1057

1058

1059

1060 **Table 4.** Summary of studies on the nitrate photolysis frequency (J<sub>nitrate</sub>) (J<sub>HNO<sub>3</sub></sub> denotes the photolysis  
 1061 frequency of gas HNO<sub>3</sub>)

Experimental conditions	Main conclusion	Reference
HNO <sub>3</sub> absorbed on Pyrex surface	J <sub>nitrate</sub> (1.2×10 <sup>-5</sup> s <sup>-1</sup> ) is 1–2 orders of magnitude faster than in the gas and aqueous phases.	(Zhou et al., 2003)
Atmosphere simulation chamber	J <sub>nitrate</sub> on snow, ground, and glass surfaces, can be excluded in the chamber.	(Rohrer et al., 2005)
HNO <sub>3</sub> absorbed on glass surface	Photolysis frequency of surfaces adsorbed HNO <sub>3</sub> is > 2 orders of magnitude larger than J <sub>HNO<sub>3</sub></sub> .	(Zhu et al., 2008)
Urban grime-coated surface	J <sub>nitrate</sub> (1.2×10 <sup>-3</sup> s <sup>-1</sup> ) is 4 orders of magnitude faster than in water (10 <sup>-7</sup> s <sup>-1</sup> ).	(Baergen and Donaldson, 2013)
Various natural/artificial surfaces	J <sub>nitrate</sub> ranges from 6.0×10 <sup>-6</sup> s <sup>-1</sup> to 3.7×10 <sup>-4</sup> s <sup>-1</sup> , 1–3 orders of magnitude higher than J <sub>HNO<sub>3</sub></sub>	(Ye et al., 2016a)
Adsorbed HNO <sub>3</sub> on glass surfaces	Photolysis frequency of surfaces adsorbed HNO <sub>3</sub> (2.4×10 <sup>-7</sup> s <sup>-1</sup> ) is very low.	(Laufs and Kleffmann, 2016)

Aerosol filter samples	$J_{\text{nitrate}}$ ranges from $6.2 \times 10^{-6} \text{ s}^{-1}$ to $5.0 \times 10^{-4} \text{ s}^{-1}$ with a mean of $1.3 \times 10^{-4} \text{ s}^{-1}$ .	(Ye et al., 2017)
Nitrate aerosol in the MBL	$J_{\text{nitrate}}$ is $\sim 10$ times higher than $J_{\text{HNO}_3}$ .	(Reed et al., 2017)
PM <sub>2.5</sub> in Beijing	$J_{\text{nitrate}}$ ( $1.22 \times 10^{-5} \text{ s}^{-1}$ to $4.84 \times 10^{-4} \text{ s}^{-1}$ ) is 1–3 orders of magnitude higher than $J_{\text{HNO}_3}$ .	(Bao et al., 2018)
Sea-salt particulate nitrate	$J_{\text{nitrate}}$ is 25–50 times higher than $J_{\text{HNO}_3}$ .	(Kasibhatla et al., 2018)
Particles collected on filters	$J_{\text{nitrate}}$ is $\leq 30$ times $J_{\text{HNO}_3}$ .	(Romer et al., 2018)
CMAQ simulation	Nitrate photolysis contributed $\sim 30\%$ of noontime HONO with a $J_{\text{nitrate}}/J_{\text{HNO}_3}$ ratio of $\sim 120$ .	(Fu et al., 2019)
CMAQ simulation	A $J_{\text{nitrate}}/J_{\text{HNO}_3}$ ratio of 100 better improved sulfate simulations than a $J_{\text{nitrate}}/J_{\text{HNO}_3}$ ratio of 10.	(Zheng et al., 2020)
MCM Box model	Nitrate photolysis contribution to HONO was $< 8\%$ with a $J_{\text{nitrate}}/J_{\text{HNO}_3}$ ratio of 30.	(Xue et al., 2020)
MCM Box model	Nitrate photolysis contributed $\sim 40\%$ of noontime HONO with a $J_{\text{nitrate}}/J_{\text{HNO}_3}$ ratio of $\sim 120$ .	(Shi et al., 2020)
Smog chamber	The $J_{\text{nitrate}}/J_{\text{HNO}_3}$ ratio was $< 10$ for suspended submicron $\text{NaNO}_3$ and $\text{NH}_4\text{NO}_3$ .	(Shi et al., 2021)
CMAQ simulation	Nitrate photolysis contribution to surface HONO was $\sim 1.0\%$ with a $J_{\text{nitrate}}/J_{\text{HNO}_3}$ ratio of 30.	(Zhang et al., 2021)
WRF-Chem simulation	The relative contribution of nitrate photolysis to HONO increased with rising altitude and nitrate photolysis contributed much larger in the ABL than near the surface to the enhanced $\text{O}_3$ . On average, nitrate photolysis contributed $\sim 5\%$ of surface daytime HONO with a $J_{\text{nitrate}}/J_{\text{HNO}_3}$ ratio of 30 ( $\sim 1 \times 10^{-5} \text{ s}^{-1}$ ) but contributed $\sim 30\text{--}50\%$ of the enhanced $\text{O}_3$ near the surface in NCP in hazy days.	This study

Deleted: the enhanced  $\text{O}_3$

Deleted: HONO

Formatted: Subscript

1063 MBL: marine boundary layer; ABL: atmospheric boundary layer.

1064

1065

1066

1067 **4.3 Interactions between heterogeneous HONO sources**

1068 Form the comparison of nitrate budget induced by the six potential HONO

1069 sources in Fig.S3&S9, we can find that  $\text{Het}_{\text{ground}}$  led to an significant increase in

1070 nitrate concentrations. In the real atmosphere, the  $\text{NO}_2$  heterogeneous reactions and

Formatted: Line spacing: Double

Deleted: 4

Deleted: The i

Deleted: the

Formatted: Font color: Text 1

Formatted: Line spacing: Double

Formatted: Font: Bold, Font color: Text 1

Formatted: Font color: Text 1

Deleted: cloud clearly

Deleted: the nitrate concentrations were increased by

Formatted: Font color: Text 1, Subscript

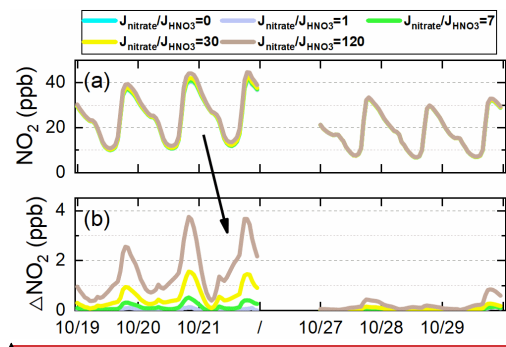
Formatted: Font color: Text 1

Formatted: Font color: Text 1, Subscript

Formatted: Font color: Text 1

1078 the  $J_{\text{nitrate}}$  reaction occur simultaneously, while the sensitivity tests only considered  
 1079 one specific HONO source for each case and neglected their interactions, leading to  
 1080 the underestimation of the  $J_{\text{nitrate}}$  impact to some extent. Take it into consideration,  
 1081 the  $J_{\text{nitrate}}$  impact on atmospheric oxidants and secondary pollutants would be even  
 1082 larger, especially during the haze aggravating process.

1083  $J_{\text{nitrate}}$  would in turn change  $\text{NO}_x$  concentrations to some extent. From the  
 1084 95-site-averaged  $\text{NO}_2$  concentrations shown in Fig. 20, we can find that  $J_{\text{nitrate}}$   
 1085 slightly increased  $\text{NO}_2$  concentrations in hazy days. The elevated  $\text{NO}_2$  concentration  
 1086 could enhance HONO formation via the  $\text{NO}_2$  heterogeneous reactions, nevertheless,  
 1087 due to the high background  $\text{NO}_2$  concentrations in NCP (up to ~ 40 ppb at nighttime),  
 1088 the increment of  $\text{NO}_2$  and the enhanced HONO formation from  $\text{NO}_2$  caused by  
 1089  $J_{\text{nitrate}}$  were small (<10%), but might have a larger impact on  $\text{NO}_x$  budgets in clean  
 1090 regions. From the above, a positive feedback relationship between the  $\text{NO}_2$   
 1091 heterogeneous reactions and the  $J_{\text{nitrate}}$  reaction could be found, these  
 1092 multi-processes worse the air quality during the haze aggravating processes.



- Deleted: nitrate photolysis
- Formatted
- Deleted: s were occurred ...ccur simultaneously, while the
- Formatted
- Deleted: impact of
- Deleted: The nitrate photolysis
- Formatted: Font: Not Italic, Font color: Text 1
- Formatted: Indent: First line: 0.74 cm, Line spacing: Double
- Formatted
- Deleted: s
- Deleted: find that nitrate photolysis
- Formatted
- Deleted: below
- Formatted
- Deleted: could
- Formatted: Font color: Text 1
- Formatted
- Deleted: e
- Formatted
- Deleted: nitrate photolysis
- Formatted
- Deleted: was
- Formatted
- Deleted: this process
- Formatted
- Deleted: to
- Formatted
- Deleted: nitrate photolysis
- Formatted
- Deleted: s
- Formatted: Font: Not Italic, Font color: Text 1
- Formatted: Font color: Text 1
- Formatted: Font color: Text 1



1131 Figure 20 Comparison of 95-site-averaged simulations of NO<sub>2</sub> concentrations for the base case and  
1132 four cases with different J<sub>nitrate</sub>/J<sub>HNO<sub>3</sub></sub> ratios (1, 7, 30 and 120) (a), and the corresponding NO<sub>2</sub> variations  
1133 (b) compared with the base case in the North China Plain during Oct.11–31 of 2018.

1134

- Deleted: 1
- Deleted: mean
- Deleted: simulated
- Deleted: the
- Deleted: added Phot<sub>nitrate</sub>
- Deleted: hourly

1141 **5. Conclusions**

1142 In this study, three direct emission sources, the improved NO<sub>2</sub> heterogeneous  
1143 reactions on aerosol and ground surfaces, and particulate nitrate photolysis in the  
1144 atmosphere were included into the WRF-Chem [model](#) to explore the key [HONO](#)  
1145 sources producing O<sub>3</sub> enhancements during typical autumn haze aggravating  
1146 processes with co-occurrence of high PM<sub>2.5</sub> and O<sub>3</sub> in NCP. The six potential HONO  
1147 sources produced a significant enhancement in surface HONO simulations and  
1148 improved the mean HONO concentration at the BUCT site to 1.47 ppb from 0.05 ppb  
1149 (improved the NMB to -14.22% from -97.11% and the IOA to 0.80 from 0.45). The  
1150 improved HONO significantly enhanced the atmospheric oxidation capacity near the  
1151 surface and at elevated heights, especially in hazy days, resulting in fast formation of  
1152 and significant improvements of O<sub>3</sub> during haze aggravating processes in NCP.  
1153 Although the photolysis frequency is usually lower during hazy days, higher  
1154 concentrations of NO<sub>2</sub>, PM<sub>2.5</sub> and nitrate favored HONO formation via heterogeneous  
1155 reactions, leading to stronger atmospheric oxidation capacity. The major results  
1156 include:

1157 (1) For the surface HONO in NCP, Het<sub>ground</sub> was the largest source during  
1158 daytime and nighttime (~50–80%); the contribution of Phot<sub>nitrate</sub> ( $J_{\text{nitrate}}/J_{\text{HNO}_3} = 30$ ) to  
1159 surface HONO concentrations was close to that of the NO+OH reaction during  
1160 daytime (~1–12%) and was ~5% for daytime average; E<sub>traffic</sub> was important during  
1161 nighttime (~10–20%) but small during daytime (<5%); the contribution of Het<sub>aerosol</sub>  
1162 was minor (~2–3%) in daytime and <10% in nighttime; the contribution of E<sub>soil</sub> was

Deleted: of HONO

Deleted: 86

Deleted: 78

1166 <3%, and  $E_{\text{indoor}}$  could be neglected. Vertically, the HONO enhancements due to  
1167 ground-based potential HONO sources ( $E_{\text{traffic}}$ ,  $E_{\text{soil}}$ ,  $E_{\text{indoor}}$  and  $H_{\text{etground}}$ ) decreased  
1168 rapidly with height, while the NO+OH reaction and aerosol-related HONO sources  
1169 ( $Phot_{\text{nitrate}}$  and  $H_{\text{et aerosol}}$ ) decreased with height much slower. The enhanced HONO  
1170 due to  $Phot_{\text{nitrate}}$  in hazy days was about ten times larger than in clean days and  
1171 became the dominant HONO source (~30–70% when  $J_{\text{nitrate}}/J_{\text{HNO}_3} = 30$ ) at higher  
1172 layers, and both HONO concentrations and  $Phot_{\text{nitrate}}$  contributions increased with the  
1173 aggravated pollution levels.

Deleted: one order of magnitude

1174 (2) Near the surface, daytime OH production/loss rates were significantly  
1175 enhanced by ~320% for the 6S case (mean was 5.27 ppb h<sup>-1</sup>) compared with the base  
1176 case (mean was 1.26 ppb h<sup>-1</sup>); vertically, daytime OH production/loss rates were  
1177 enhanced by ~105% for the 6S case (mean was 2.21 ppb h<sup>-1</sup>) compared with the base  
1178 case (mean was 1.08 ppb h<sup>-1</sup>). The enhanced OH production rate and OH due to the  
1179 six potential HONO sources both showed a strong positive correlation with PM<sub>2.5</sub>  
1180 concentrations at the 95 NCP sites, with a slope of 0.043 ppb h<sup>-1</sup>/μg m<sup>-3</sup> of PM<sub>2.5</sub> and  
1181  $3.62 \times 10^4$  molec cm<sup>-3</sup>/μg m<sup>-3</sup> of PM<sub>2.5</sub> from the surface to the height of 2.5 km for case  
1182 6S, respectively. The atmospheric oxidation capacity (e.g., OH) was enhanced in the  
1183 haze aggravating process.

1184 (3) A strong positive correlation ( $r > 0.8$ ) between enhanced O<sub>3</sub> by the six potential  
1185 HONO sources and PM<sub>2.5</sub> concentrations was found in NCP, and nitrate photolysis  
1186 was the largest contributor to the enhanced DMA8 O<sub>3</sub> in hazy days. Vertically, the  
1187 enhanced DMA8 O<sub>3</sub> was < 2ppb when PM<sub>2.5</sub> was < 20μg m<sup>-3</sup>, and that was >10 ppb

1189 when  $PM_{2.5}$  was  $> 60\mu\text{g m}^{-3}$  on average, with a slope of 0.24 ppb DMA8  $O_3$   
1190 enhancement  $/\mu\text{g m}^{-3}$  of  $PM_{2.5}$ . The surface enhanced DMA8  $O_3$  was  $\sim 5.5$  ppb  
1191 (Oct.19),  $\sim 7$  ppb (Oct.20) and  $\sim 10$  ppb (Oct.21), respectively, during a typical haze  
1192 aggravating process, while that was usually  $\sim 2$  ppb in clean days. The contribution of  
1193  $Phot_{\text{nitrate}}$  to the enhanced DMA8  $O_3$  was increased by over one magnitude during the  
1194 haze aggravating process (up to 5–10 ppb) compared with that in clean days ( $\sim 0.1$ – $0.5$   
1195 ppb), reached  $\sim 2$ – $4.5$  ppb (Oct.19),  $\sim 3$ – $6$  ppb (Oct.20) and  $\sim 5$ – $10$  ppb (Oct.21),  
1196 respectively, during a typical haze aggravating process vertically.

Deleted: and

1197 (4) Surface  $O_3$  was controlled by VOCs-sensitive chemistry, while  $O_3$  at higher  
1198 altitude ( $>800\text{m}$ ) was controlled by  $NO_x$ -sensitive chemistry in NCP during autumn.  
1199 The nitrate photolysis reaction enhanced OH and  $NO_x$  concentrations, both favored  $O_3$   
1200 formation at high altitude, especially in haze aggravating processes with abundant  
1201 nitrate. The produced HONO rather than the produced  $NO_2$  through nitrate photolysis  
1202 had a stronger promotion for  $O_3$  formation near the surface, but the impacts of the two  
1203 products on  $O_3$  enhancements were similar at higher altitude ( $\sim 2000$  m).

1204 (5) Nitrate photolysis only contributed  $\sim 5\%$  of the surface HONO in daytime  
1205 with a  $J_{\text{nitrate}}/J_{\text{HNO}_3}$  ratio of 30 ( $\sim 1 \times 10^{-5} \text{ s}^{-1}$ ) but contributed  $\sim 30$ – $50\%$  of the enhanced  
1206  $O_3$  near the surface in NCP in hazy days. The photolysis of nitrate had a limited  
1207 impact on nitrate concentrations (reduced by  $<5\%$  with  $J_{\text{nitrate}}/J_{\text{HNO}_3} = 30$ , and  $<15\%$   
1208 even with a  $J_{\text{nitrate}}/J_{\text{HNO}_3}$  ratio of 120), due mainly to the simultaneously enhanced  
1209 atmospheric oxidants favoring the formation of  $HNO_3$  and nitrate. Choosing a larger  
1210  $J_{\text{nitrate}}$  value might cover up other ground-based unknown HONO sources, but

Deleted: oxidation

Deleted:

Deleted: formation

Formatted: Subscript

1215 overestimate vertical sources of HONO, and NO<sub>x</sub> and O<sub>3</sub> concentrations, so more  
1216 studies are still needed to find the exact value of J<sub>nitrate</sub> in the real atmosphere.

1217

#### 1218 **Data availability**

1219 Data are available upon reasonable request to the corresponding authors.

1220

#### 1221 **Author contribution:**

1222 J.Z., C.L., J.A., M.G., and W.W. conceived and designed the research. J.Z. performed

1223 WRF-Chem simulations and wrote the paper. J.Z., C.L., Y.G., and H.R. performed

Deleted: and analyzed

1224 data analyses and produced the figures. C.L., Y.Z., F.Z., X.F., C.Y., K.D., Y.L., and

1225 M.K. conducted the field observations. W.W., J.A., M.G., Y.L., and M.K. reviewed the

Deleted: .

1226 article.

#### 1227 **Competing interests**

1228 The authors declare that they have no conflict of interest.

1229

#### 1230 **Acknowledgements**

1231 This research was partially supported by the National Natural Science Foundation of

1232 China (Grant No. 92044302, 42075108, 42107124, [42075110](#), 41822703, 91544221,

1233 91844301), Beijing National Laboratory for Molecular Sciences

1236 (BNLMS-CXXM-202011) and the China Postdoctoral Science Foundation (grant NO.

1237 2019M660764).

1238

1239 **References**

- 1240 Aliche, B., Platt, U., Stutz, J., 2002. Impact of nitrous acid photolysis on the total hydroxyl radical  
 1241 budget during the Limitation of Oxidant Production/Pianura Padana Produzione di Ozono study in  
 1242 Milan. *J Geophys Res-Atmos* 107. doi:10.1029/2000JD000075.
- 1243 An, J.L., Li, Y., Chen, Y., Li, J., Qu, Y., Tang, Y.J., 2013. Enhancements of major aerosol components  
 1244 due to additional HONO sources in the North China Plain and implications for visibility and haze.  
 1245 *Advances in Atmospheric Sciences* 30, 57-66.
- 1246 [Aumont, B., Chervier, F., Laval, S., 2003. Contribution of HONO sources to the NO<sub>x</sub>/HO<sub>x</sub>/O<sub>3</sub>  
 1247 chemistry in the polluted boundary layer. \*Atmospheric Environment\* 37, 487-498.](#)
- 1248 Avnery, S., Mauzerall, D.L., Liu, J., Horowitz, L.W., 2011a. Global crop yield reductions due to surface  
 1249 ozone exposure: 1. Year 2000 crop production losses and economic damage. *Atmospheric*  
 1250 *Environment* 45, 2284-2296.
- 1251 Avnery, S., Mauzerall, D.L., Liu, J., Horowitz, L.W., 2011b. Global crop yield reductions due to  
 1252 surface ozone exposure: 2. Year 2030 potential crop production losses and economic damage  
 1253 under two scenarios of O<sub>3</sub> pollution. *Atmospheric Environment* 45, 2297-2309.
- 1254 Baergen, A.M., Donaldson, D.J., 2013. Photochemical renoxification of nitric acid on real urban grime.  
 1255 *Environmental Science & Technology* 47, 815-820.
- 1256 Bao, F., Li, M., Zhang, Y., Chen, C., Zhao, J., 2018. Photochemical Aging of Beijing Urban PM<sub>2.5</sub>:  
 1257 HONO Production. *Environmental Science & Technology* 52, 6309-6316.
- 1258 Bao, F.X., Jiang, H.Y., Zhang, Y., Li, M., Ye, C.X., Wang, W.G., Ge, M.F., Chen, C.C., Zhao, J.C., 2020.  
 1259 The Key Role of Sulfate in the Photochemical Renoxification on Real PM<sub>2.5</sub>. *Environmental*  
 1260 *Science & Technology* 54, 3121-3128.
- 1261 [Bejan, I., Abd-el-Aal, Y., Barnes, I., Benter, T., Bohn, B., Wiesen, P., Kleffmann, J., 2006. The  
 1262 photolysis of ortho-nitrophenols: a new gas phase source of HONO. \*Physical chemistry chemical\*  
 1263 \*physics : PCCP\* 8, 2028-2035.](#)
- 1264 Chen, S., Wang, H., Lu, K., Zeng, L., Hu, M., Zhang, Y., 2020a. The trend of surface ozone in Beijing  
 1265 from 2013 to 2019: Indications of the persisting strong atmospheric oxidation capacity.  
 1266 *Atmospheric Environment* 242, 117801.
- 1267 Chen, Y., Wang, W.G., Lian, C.F., Peng, C., Zhang, W.Y., Li, J.L., Liu, M.Y., Shi, B., Wang, X.F., Ge,  
 1268 M.F., 2020b. Evaluation and impact factors of indoor and outdoor gas-phase nitrous acid under  
 1269 different environmental conditions. *Journal of Environmental Sciences* 95, 165-171.
- 1270 [Chen, Y., Zheng, P., Wang, Z., Pu, W., Tan, Y., Yu, C., Xia, M., Wang, W., Guo, J., Huang, D., Yan, C.,  
 1271 Nie, W., Ling, Z., Chen, Q., Lee, S., Wang, T., 2021. Secondary Formation and Impacts of  
 1272 Gaseous Nitro-Phenolic Compounds in the Continental Outflow Observed at a Background Site in  
 1273 South China. \*Environmental Science & Technology\*. DOI: 10.1021/acs.est.1c04596.](#)
- 1274 [Crowley, J.N., Carl, S.A., 1997. OH formation in the photoexcitation of NO<sub>2</sub> beyond the dissociation  
 1275 threshold in the presence of water vapor. \*Journal of Physical Chemistry A\* 101, 4178-4184.](#)
- 1276 Cui, L., Li, R., Fu, H., Meng, Y., Zhao, Y., Li, Q., Chen, J., 2021. Nitrous acid emission from open  
 1277 burning of major crop residues in mainland China. *Atmospheric Environment* 244, 117950.
- 1278 [Dillon, T.J., Crowley, J.N., 2018. Reactive quenching of electronically excited NO<sub>x</sub><sup>\\*</sup> and NO<sub>x</sub><sup>\\*</sup> by H<sub>2</sub>O  
 1279 as potential sources of atmospheric HO<sub>x</sub> radicals. \*Atmospheric Chemistry and Physics\* 18,  
 1280 14005-14015.](#)

Formatted: Subscript

Formatted: Subscript

Formatted: Subscript

Formatted: Subscript

Formatted: Superscript

Formatted: Subscript

Formatted: Superscript

Formatted: Subscript

Formatted: Subscript

- 1281 Dong, W., Xing, J., Wang, S., 2010. Temporal and spatial distribution of anthropogenic ammonia  
1282 emissions in China: 1994-2006. *Environmental Sciences (in Chinese)* 31, 1457-1463.
- 1283 [Emmons, L.K., Walters, S., Hess, P.G., Lamarque, J.F., Pfister, G.G., Fillmore, D., Granier, C.,](#)  
1284 [Guenther, A., Kinnison, D., Laepple, T., Orlando, J., Tie, X., Tyndall, G., Wiedinmyer, C.,](#)  
1285 [Baughcum, S.L., Kloster, S., 2010. Description and evaluation of the Model for Ozone and](#)  
1286 [Related chemical Tracers, version 4 \(MOZART-4\). \*Geoscientific Model Development\* 3, 43-67.](#)
- 1287 Feng, T., Zhao, S., Bei, N., Liu, S., Li, G., 2021. Increasing atmospheric oxidizing capacity weakens  
1288 emission mitigation effort in Beijing during autumn haze events. *Chemosphere* 281, 130855.
- 1289 Feng, Z., De Marco, A., Anav, A., Gualtieri, M., Sicard, P., Tian, H., Formasier, F., Tao, F., Guo, A.,  
1290 Paoletti, E., 2019. Economic losses due to ozone impacts on human health, forest productivity and  
1291 crop yield across China. *Environ Int* 131, 104966.
- 1292 Feng, Z., Hu, E., Wang, X., Jiang, L., Liu, X., 2015. Ground-level O<sub>3</sub> pollution and its impacts on food  
1293 crops in China: a review. *Environ Pollut* 199, 42-48.
- 1294 [Feng, Z., Xu, Y., Kobayashi, K., Dai, L., Zhang, T., Agathokleous, E., Calatayud, V., Paoletti, E.,](#)  
1295 [Mukherjee, A., Agrawal, M., Park, R.J., Oak, Y.J., Yue, X., 2022. Ozone pollution threatens the](#)  
1296 [production of major staple crops in East Asia. \*Nature Food\* 3, 47-56.](#)
- 1297 Finlayson-Pitts, B.J., Wingen, L.M., Sumner, A.L., Syomin, D., Ramazan, K.A., 2003. The  
1298 heterogeneous hydrolysis of NO<sub>2</sub> in laboratory systems and in outdoor and indoor atmospheres:  
1299 An integrated mechanism. *Physical Chemistry Chemical Physics* 5, 223-242.
- 1300 [Fröhlich, R., Cubison, M.J., Slowik, J.G., Bukowiecki, N., Prévôt, A.S.H., Baltensperger, U., Schneider,](#)  
1301 [J., Kimmel, J.R., Gonin, M., Rohner, U., Worsnop, D.R., Jayne, J.T., 2013. The ToF-ACSM: a](#)  
1302 [portable aerosol chemical speciation monitor with TOFMS detection. \*Atmospheric Measurement\*](#)  
1303 [Techniques 6, 3225-3241.](#)
- 1304 Fu, X., Wang, T., Gao, J., Wang, P., Liu, Y.M., Wang, S.X., Zhao, B., Xue, L.K., 2020. Persistent Heavy  
1305 Winter Nitrate Pollution Driven by Increased Photochemical Oxidants in Northern China.  
1306 *Environmental Science & Technology* 54, 3881-3889.
- 1307 Fu, X., Wang, T., Zhang, L., Li, Q.Y., Wang, Z., Xia, M., Yun, H., Wang, W.H., Yu, C., Yue, D.L., Zhou,  
1308 Y., Zheng, J.Y., Han, R., 2019. The significant contribution of HONO to secondary pollutants  
1309 during a severe winter pollution event in southern China. *Atmospheric Chemistry and Physics* 19,  
1310 1-14.
- 1311 Gao, W., Tan, G., Hong, Y., Li, M., Nian, H., Guo, C., Huang, Z., Fu, Z., Dong, J., Xu, X., 2013.  
1312 Development of portable single photon ionization time-of-flight mass spectrometer combined with  
1313 membrane inlet. *International Journal of Mass Spectrometry* 334, 8-12.
- 1314 Ge, M., Tong, S., Wang, W., Zhang, W., Chen, M., Peng, C., Li, J., Zhou, L., Chen, Y., Liu, M., 2021.  
1315 Important Oxidants and Their Impact on the Environmental Effects of Aerosols. *The journal of*  
1316 *physical chemistry. A* 125, 3813-3825.
- 1317 Ge, S., Wang, G., Zhang, S., Li, D., Xie, Y., Wu, C., Yuan, Q., Chen, J., Zhang, H., 2019. Abundant  
1318 NH<sub>3</sub> in China Enhances Atmospheric HONO Production by Promoting the Heterogeneous  
1319 Reaction of SO<sub>2</sub> with NO<sub>2</sub>. *Environmental Science & Technology* 53, 14339-14347.
- 1320 [Gen, M., Liang, Z., Zhang, R., Go Mabato, B.R., Chan, C.K., 2022. Particulate nitrate photolysis in the](#)  
1321 [atmosphere. \*Environmental Science: Atmospheres\*. DOI: 10.1039/D1EA00087J.](#)
- 1322 Gligorovski, S., Strekowski, R., Barabati, S., Vione, D., 2015. Environmental Implications of Hydroxyl  
1323 Radicals (\*OH). *Chem Rev* 115, 13051-13092.
- 1324 Gómez Alvarez, E., Sörgel, M., Gligorovski, S., Bassil, S., Bartolomei, V., Coulomb, B., Zetzsch, C.,

Formatted: Normal, Indent: Left: 0 cm, Hanging: 4.2 ch,  
First line: 0 ch

Formatted: Normal, Indent: Left: 0 cm, Hanging: 4.2 ch,  
First line: 0 ch



1325 Wortham, H., 2014. Light-induced nitrous acid (HONO) production from NO<sub>2</sub> heterogeneous  
1326 reactions on household chemicals. *Atmospheric Environment* 95, 391-399.

1327 Guenther, A.B., Jiang, X., Heald, C.L., Sakulyanontvittaya, T., Duhl, T., Emmons, L.K., Wang, X.,  
1328 2012. The Model of Emissions of Gases and Aerosols from Nature version 2.1 (MEGAN2.1): an  
1329 extended and updated framework for modeling biogenic emissions. *Geoscientific Model*  
1330 *Development* 5, 1471-1492.

1331 Guo, Y., Zhang, J., An, J., Qu, Y., Liu, X., Sun, Y., Chen, Y., 2020. Effect of vertical parameterization of  
1332 a missing daytime source of HONO on concentrations of HONO, O<sub>3</sub> and secondary organic  
1333 aerosols in eastern China. *Atmospheric Environment* 226, 117208.

1334 Hendrick, F., Muller, J.F., Clemer, K., Wang, P., De Maziere, M., Fayt, C., Gielen, C., Hermans, C., Ma,  
1335 J.Z., Pinardi, G., Stavrou, T., Vlemmix, T., Van Roozendaal, M., 2014. Four years of  
1336 ground-based MAX-DOAS observations of HONO and NO<sub>2</sub> in the Beijing area. *Atmospheric*  
1337 *Chemistry and Physics* 14, 765-781.

1338 Huang, X., Li, M.M., Li, J.F., Song, Y., 2012. A high-resolution emission inventory of crop burning in  
1339 fields in China based on MODIS Thermal Anomalies/Fire products. *Atmospheric Environment* 50,  
1340 9-15.

1341 Kasibhatla, P., Sherwen, T., Evans, M.J., Carpenter, L.J., Reed, C., Alexander, B., Chen, Q.J., Sulprizio,  
1342 M.P., Lee, J.D., Read, K.A., Bloss, W., Crilley, L.R., Keene, W.C., Pszenny, A.A.P., Hodzic, A.,  
1343 2018. Global impact of nitrate photolysis in sea-salt aerosol on NO<sub>x</sub>, OH, and O<sub>3</sub> in the marine  
1344 boundary layer. *Atmospheric Chemistry and Physics* 18, 11185-11203.

1345 Kim, S., VandenBoer, T.C., Young, C.J., Riedel, T.P., Thornton, J.A., Swarthout, B., Sive, B., Lerner, B.,  
1346 Gilman, J.B., Warneke, C., Roberts, J.M., Guenther, A., Wagner, N.L., Dube, W.P., Williams, E.,  
1347 Brown, S.S., 2014. The primary and recycling sources of OH during the NACHTT-2011  
1348 campaign: HONO as an important OH primary source in the wintertime. *J Geophys Res-Atmos*  
1349 119, 6886-6896.

1350 Kleffmann, J., Kurtenbach, R., Lorzer, J., Wiesen, P., Kalthoff, N., Vogel, B., Vogel, H., 2003.  
1351 Measured and simulated vertical profiles of nitrous acid - Part I: Field measurements.  
1352 *Atmospheric Environment* 37, 2949-2955.

1353 Klosterkother, A., Kurtenbach, R., Wiesen, P., Kleffmann, J., 2021. Determination of the emission  
1354 indices for NO, NO<sub>2</sub>, HONO, HCHO, CO, and particles emitted from candles. *Indoor Air* 31,  
1355 116-127.

1356 Kramer, L.J., Crilley, L.R., Adams, T.J., Ball, S.M., Pope, F.D., Bloss, W.J., 2020. Nitrous acid (HONO)  
1357 emissions under real-world driving conditions from vehicles in a UK road tunnel. *Atmospheric*  
1358 *Chemistry and Physics* 20, 5231-5248.

1359 Kubota, M., Asami, T., 1985. Volatilization of Nitrous-Acid from Upland Soils. *Soil Science and Plant*  
1360 *Nutrition* 31, 27-34.

1361 Kurtenbach, R., Becker, K.H., Gomes, J.A.G., Kleffmann, J., Lorzer, J.C., Spittler, M., Wiesen, P.,  
1362 Ackermann, R., Geyer, A., Platt, U., 2001. Investigations of emissions and heterogeneous  
1363 formation of HONO in a road traffic tunnel. *Atmospheric Environment* 35, 3385-3394.

1364 Laufs, S., Kleffmann, J., 2016. Investigations on HONO formation from photolysis of adsorbed HNO<sub>3</sub>  
1365 on quartz glass surfaces. *Physical Chemistry Chemical Physics* 18, 9616-9625.

1366 [Lee, J.D., Whalley, L.K., Heard, D.E., Stone, D., Dunmore, R.E., Hamilton, J.F., Young, D.E., Allan,](#)  
1367 [J.D., Laufs, S., Kleffmann, J., 2016. Detailed budget analysis of HONO in central London reveals](#)  
1368 [a missing daytime source. Atmospheric Chemistry and Physics 16, 2747-2764.](#)

- 1369 Li, G., Lei, W., Zavala, M., Volkamer, R., Dusanter, S., Stevens, P., Molina, L.T., 2010. Impacts of  
1370 HONO sources on the photochemistry in Mexico City during the MCMA-2006/MILAGO  
1371 Campaign. *Atmospheric Chemistry and Physics* 10, 6551-6567.
- 1372 Li, K., Jacob, D.J., Shen, L., Lu, X., De Smedt, I., Liao, H., 2020. Increases in surface ozone pollution  
1373 in China from 2013 to 2019: anthropogenic and meteorological influences. *Atmospheric*  
1374 *Chemistry and Physics* 20, 11423-11433.
- 1375 Li, L., Chen, C.H., Huang, C., Huang, H.Y., Zhang, G.F., Wang, Y.J., Wang, H.L., Lou, S.R., Qiao, L.P.,  
1376 Zhou, M., Chen, M.H., Chen, Y.R., Streets, D.G., Fu, J.S., Jang, C.J., 2012. Process analysis of  
1377 regional ozone formation over the Yangtze River Delta, China using the Community Multi-scale  
1378 Air Quality modeling system. *Atmospheric Chemistry and Physics* 12, 10971-10987.
- 1379 Li, M., Zhang, Q., Kurokawa, J., Woo, J.H., He, K.B., Lu, Z.F., Ohara, T., Song, Y., Streets, D.G.,  
1380 Carmichael, G.R., Cheng, Y.F., Hong, C.P., Huo, H., Jiang, X.J., Kang, S.C., Liu, F., Su, H., Zheng,  
1381 B., 2017. MIX: a mosaic Asian anthropogenic emission inventory under the international  
1382 collaboration framework of the MICS-Asia and HTAP. *Atmospheric Chemistry and Physics* 17,  
1383 935-963.
- 1384 [Li, S., Matthews, J., Sinha, A., 2008. Atmospheric hydroxyl radical production from electronically](#)  
1385 [excited NO<sub>2</sub> and H<sub>2</sub>O. \*Science\* 319, 1657-1660.](#)
- 1386 [Li, X., Rohrer, F., Hofzumahaus, A., Brauers, T., Häsel, R., Bohn, B., Broch, S., Fuchs, H., Gomm, S.,](#)  
1387 [Holland, F., 2015. Response to Comment on “Missing gas-phase source of HONO inferred from](#)  
1388 [Zeppelin measurements in the troposphere”. \*Science\* 348, 1326-1326.](#)
- 1389 [Li, X., Rohrer, F., Hofzumahaus, A., Brauers, T., Haseler, R., Bohn, B., Broch, S., Fuchs, H., Gomm, S.,](#)  
1390 [Holland, F., Jäger, J., Kaiser, J., Keutsch, F.N., Lohse, I., Lu, K., Tillmann, R., Wegener, R., Wolfe,](#)  
1391 [G.M., Mentel, T.F., Kiendler-Scharr, A., Wahner, A., 2014. Missing gas-phase source of HONO](#)  
1392 [inferred from Zeppelin measurements in the troposphere. \*Science\* 344, 292-296.](#)
- 1393 Li, Y., An, J.L., Min, M., Zhang, W., Wang, F., Xie, P.H., 2011. Impacts of HONO sources on the air  
1394 quality in Beijing, Tianjin and Hebei Province of China. *Atmospheric Environment* 45,  
1395 4735-4744.
- 1396 Liao, S., Zhang, J., Yu, F., Zhu, M., Liu, J., Ou, J., Dong, H., Sha, Q., Zhong, Z., Xie, Y., Luo, H.,  
1397 Zhang, L., Zheng, J., 2021. High Gaseous Nitrous Acid (HONO) Emissions from Light-Duty  
1398 Diesel Vehicles. *Environmental science & technology* 55, 200-208.
- 1399 Lin, Y.L., Farley, R.D., Orville, H.D., 1983. Bulk Parameterization of the Snow Field in a Cloud Model.  
1400 *J Clim Appl Meteorol* 22, 1065-1092.
- 1401 Liu, J., Li, S., Zeng, J., Mekic, M., Yu, Z., Zhou, W., Loisel, G., Gandolfo, A., Song, W., Wang, X.,  
1402 Zhou, Z., Herrmann, H., Li, X., Gligorovski, S., 2019. Assessing indoor gas phase oxidation  
1403 capacity through real-time measurements of HONO and NO<sub>x</sub> in Guangzhou, China. *Environ Sci*  
1404 *Process Impacts* 21, 1393-1402.
- 1405 [Liu, Y., Zhang, Y., Lian, C., Yan, C., Feng, Z., Zheng, F., Fan, X., Chen, Y., Wang, W., Chu, B., Wang,](#)  
1406 [Y., Cai, J., Du, W., Daellenbach, K.R., Kangasluoma, J., Bianchi, F., Kujansuu, J., Petäjä, T., Wang,](#)  
1407 [X., Hu, B., Wang, Y., Ge, M., He, H., Kulmala, M., 2020. The promotion effect of nitrous acid on](#)  
1408 [aerosol formation in wintertime in Beijing: the possible contribution of traffic-related emissions.](#)  
1409 [\*Atmospheric Chemistry and Physics\* 20, 13023-13040.](#)
- 1410 Liu, Z., Wang, Y., Costabile, F., Amoroso, A., Zhao, C., Huey, L.G., Stickel, R., Liao, J., Zhu, T., 2014.  
1411 Evidence of aerosols as a media for rapid daytime HONO production over China. *Environmental*  
1412 *Science & Technology* 48, 14386-14391.

Formatted: Subscript

Formatted: Subscript

1413 Lu, X., Zhang, L., Wang, X.L., Gao, M., Li, K., Zhang, Y.Z., Yue, X., Zhang, Y.H., 2020. Rapid  
1414 Increases in Warm-Season Surface Ozone and Resulting Health Impact in China Since 2013.  
1415 Environmental Science & Technology Letters 7, 240-247.

1416 Ma, J., Liu, Y., Han, C., Ma, Q., Liu, C., He, H., 2013. Review of heterogeneous photochemical  
1417 reactions of  $\text{NO}_x$  on aerosol — A possible daytime source of nitrous acid (HONO) in the  
1418 atmosphere. Journal of Environmental Sciences 25, 326-334.

1419 Ma, Z.Q., Xu, J., Quan, W.J., Zhang, Z.Y., Lin, W.L., Xu, X.B., 2016. Significant increase of surface  
1420 ozone at a rural site, north of eastern China. Atmospheric Chemistry and Physics 16, 3969-3977.

1421 Maji, K.J., Namdeo, A., 2021. Continuous increases of surface ozone and associated premature  
1422 mortality growth in China during 2015-2019. Environ Pollut 269, 116183.

1423 Marion, A., Morin, J., Gandolfo, A., Ormeno, E., D'Anna, B., Wortham, H., 2021. Nitrous acid  
1424 formation on Zea mays leaves by heterogeneous reaction of nitrogen dioxide in the laboratory.  
1425 Environ Res 193, 110543.

1426 Meng, F.H., Qin, M., Tang, K., Duan, J., Fang, W., Liang, S.X., Ye, K.D., Xie, P.H., Sun, Y.L., Xie,  
1427 C.H., Ye, C.X., Fu, P.Q., Liu, J.G., Liu, W.Q., 2020. High-resolution vertical distribution and  
1428 sources of HONO and  $\text{NO}_2$  in the nocturnal boundary layer in urban Beijing, China. Atmospheric  
1429 Chemistry and Physics 20, 5071-5092.

1430 Mills, G., Buse, A., Gimeno, B., Bermejo, V., Holland, M., Emberson, L., Pleijel, H., 2007. A synthesis  
1431 of AOT40-based response functions and critical levels of ozone for agricultural and horticultural  
1432 crops. Atmospheric Environment 41, 2630-2643.

1433 Mills, G., Sharps, K., Simpson, D., Pleijel, H., Broberg, M., Uddling, J., Jaramillo, F., Davies, W.J.,  
1434 Dentener, F., Van den Berg, M., Agrawal, M., Agrawal, S.B., Ainsworth, E.A., Buker, P.,  
1435 Emberson, L., Feng, Z., Harmens, H., Hayes, F., Kobayashi, K., Paoletti, E., Van Dingenen, R.,  
1436 2018. Ozone pollution will compromise efforts to increase global wheat production. Glob Chang  
1437 Biol 24, 3560-3574.

1438 Oswald, R., Behrendt, T., Ermel, M., Wu, D., Su, H., Cheng, Y., Breuninger, C., Moravek, A., Mougín,  
1439 E., Delon, C., Loubet, B., Pommerening-Roser, A., Sorgel, M., Poschl, U., Hoffmann, T., Andreae,  
1440 M.O., Meixner, F.X., Trebs, I., 2013. HONO emissions from soil bacteria as a major source of  
1441 atmospheric reactive nitrogen. Science 341, 1233-1235.

1442 [Pagsberg, P., Bjergbakke, E., Ratajczak, E., Silleesen, A., 1997. Kinetics of the gas phase reaction](#)  
1443 [OH+NO \(+M\)->HONO \(+M\) and the determination of the UV absorption cross sections of](#)  
1444 [HONO. Chemical Physics Letters 272, 383-390.](#)

1445 Perner, D., Platt, U., 1979. Detection of nitrous acid in the atmosphere by differential optical absorption.  
1446 Geophysical Research Letters 6, 917-920.

1447 Pitts, J.N., Wallington, T.J., Biermann, H.W., Winer, A.M., 1985. Identification and Measurement of  
1448 Nitrous-Acid in an Indoor Environment. Atmospheric Environment 19, 763-767.

1449 [Qu, Y., Chen, Y., Liu, X., Zhang, J., Guo, Y., An, J., 2019. Seasonal effects of additional HONO sources](#)  
1450 [and the heterogeneous reactions of  \$\text{N}\_2\text{O}\_5\$  on nitrate in the North China Plain. The Science of the](#)  
1451 [total environment 690, 97-107.](#)

1452 Reed, C., Evans, M.J., Crilley, L.R., Bloss, W.J., Sherwen, T., Read, K.A., Lee, J.D., Carpenter, L.J.,  
1453 2017. Evidence for renoxification in the tropical marine boundary layer. Atmospheric Chemistry  
1454 and Physics 17, 4081-4092.

1455 Richards, B.L., Middleton, J.T., Hewitt, W.B., 1958. Air Pollution With Relation to Agronomic Crops:  
1456 V. Oxidant Stipple of Grape. Agronomy Journal 50, 559-561.

Formatted: Subscript

Formatted: Subscript

Formatted: Subscript

1457 Rohrer, F., Bohn, B., Brauers, T., Bruning, D., Johnen, F.J., Wahner, A., Kleffmann, J., 2005.  
1458 Characterisation of the photolytic HONO-source in the atmosphere simulation chamber SAPHIR.  
1459 Atmospheric Chemistry and Physics 5, 2189-2201.

1460 Romer, P.S., Wooldridge, P.J., Crounse, J.D., Kim, M.J., Wennberg, P.O., Dibb, J.E., Scheuer, E., Blake,  
1461 D.R., Meinardi, S., Brosius, A.L., Thames, A.B., Miller, D.O., Brune, W.H., Hall, S.R., Ryerson,  
1462 T.B., Cohen, R.C., 2018. Constraints on Aerosol Nitrate Photolysis as a Potential Source of  
1463 HONO and  $\text{NO}_x$ . *Environmental Science & Technology* 52, 13738-13746.

1464 Rondon, A., Sanhueza, E., 1989. High HONO atmospheric concentrations during vegetation burning in  
1465 the tropical savannah. *Tellus Ser. B-Chem. Phys. Meteorol.* 41, 474-477.

1466 Ryan, R.G., Rhodes, S., Tully, M., Wilson, S., Jones, N., Friess, U., Schofield, R., 2018. Daytime  
1467 HONO,  $\text{NO}_2$  and aerosol distributions from MAX-DOAS observations in Melbourne.  
1468 Atmospheric Chemistry and Physics 18, 13969-13985.

1469 [Saliba, N.A., Mochida, M., Finlayson-Pitts, B.J., 2000. Laboratory studies of sources of HONO in  
1470 polluted urban atmospheres. \*Geophysical Research Letters\* 27, 3229-3232.](#)

1471 Sakamaki, F., Hatakeyama, S., Akimoto, H., 1983. Formation of Nitrous-Acid and Nitric-Oxide in the  
1472 Heterogeneous Dark Reaction of Nitrogen-Dioxide and Water-Vapor in a Smog Chamber.  
1473 *International Journal of Chemical Kinetics* 15, 1013-1029.

1474 Sarwar, G., Roselle, S.J., Mathur, R., Appel, W., Dennis, R.L., Vogel, B., 2008. A comparison of  
1475 CMAQ HONO predictions with observations from the northeast oxidant and particle study.  
1476 *Atmospheric Environment* 42, 5760-5770.

1477 Selin, N.E., Wu, S., Nam, K.M., Reilly, J.M., Paltsev, S., Prinn, R.G., Webster, M.D., 2009. Global  
1478 health and economic impacts of future ozone pollution. *Environmental Research Letters* 4,  
1479 044014.

1480 Shi, Q., Tao, Y., Krechmer, J.E., Heald, C.L., Murphy, J.G., Kroll, J.H., Ye, Q., 2021. Laboratory  
1481 Investigation of Renoxification from the Photolysis of Inorganic Particulate Nitrate.  
1482 *Environmental science & technology*. 55, 854–861.

1483 Shi, X., Ge, Y., Zheng, J., Ma, Y., Ren, X., Zhang, Y., 2020. Budget of nitrous acid and its impacts on  
1484 atmospheric oxidative capacity at an urban site in the central Yangtze River Delta region of China.  
1485 *Atmospheric Environment* 238, 117725.

1486 Sillman, S., 1995. The use of  $\text{NO}_y$ ,  $\text{H}_2\text{O}_2$ , and  $\text{HNO}_3$  as indicators for ozone- $\text{NO}_x$ -hydrocarbon  
1487 sensitivity in urban locations. *Journal of Geophysical Research: Atmospheres* 100, 14175-14188.

1488 Slater, E.J., Whalley, L.K., Woodward-Massey, R., Ye, C.X., Lee, J.D., Squires, F., Hopkins, J.R.,  
1489 Dunmore, R.E., Shaw, M., Hamilton, J.F., Lewis, A.C., Crilley, L.R., Kramer, L., Bloss, W., Vu, T.,  
1490 Sun, Y.L., Xu, W.Q., Yue, S.Y., Ren, L.J., Acton, W.J.F., Hewitt, C.N., Wang, X.M., Fu, P.Q.,  
1491 Heard, D.E., 2020. Elevated levels of OH observed in haze events during wintertime in central  
1492 Beijing. *Atmospheric Chemistry and Physics* 20, 14847-14871.

1493 Sorgel, M., Trebs, I., Serafimovich, A., Moravek, A., Held, A., Zetzsch, C., 2011. Simultaneous HONO  
1494 measurements in and above a forest canopy: influence of turbulent exchange on mixing ratio  
1495 differences. *Atmospheric Chemistry and Physics* 11, 841-855.

1496 [Stuhl, F., Niki, H., 1972. Flash Photochemical Study of the Reaction  \$\text{OH}+\text{NO}+\text{M}\$  Using Resonance  
1497 Fluorescent Detection of OH. \*The Journal of Chemical Physics\* 57, 3677-3679.](#)

1498 Tan, Z.F., Rohrer, F., Lu, K.D., Ma, X.F., Bohn, B., Broch, S., Dong, H.B., Fuchs, H., Gkatzelis, G.I.,  
1499 Hofzumahaus, A., Holland, F., Li, X., Liu, Y., Liu, Y.H., Novelli, A., Shao, M., Wang, H.C., Wu,  
1500 Y.S., Zeng, L.M., Hu, M., Kiendler-Scharr, A., Wahner, A., Zhang, Y.H., 2018. Wintertime

Formatted: Subscript

Deleted: .

- photochemistry in Beijing: observations of RO<sub>x</sub> radical concentrations in the North China Plain during the BEST-ONE campaign. *Atmospheric Chemistry and Physics* 18, 12391-12411.
- Tang, M.J., Huang, X., Lu, K.D., Ge, M.F., Li, Y.J., Cheng, P., Zhu, T., Ding, A.J., Zhang, Y.H., Gligorovski, S., Song, W., Ding, X., Bi, X.H., Wang, X.M., 2017. Heterogeneous reactions of mineral dust aerosol: implications for tropospheric oxidation capacity. *Atmospheric Chemistry and Physics* 17, 11727-11777.
- Tang, Y., An, J., Wang, F., Li, Y., Qu, Y., Chen, Y., Lin, J., 2015. Impacts of an unknown daytime HONO source on the mixing ratio and budget of HONO, and hydroxyl, hydroperoxyl, and organic peroxy radicals, in the coastal regions of China. *Atmospheric Chemistry and Physics* 15, 9381-9398.
- Theys, N., Volkamer, R., Mueller, J.F., Zarzana, K.J., Kille, N., Clarisse, L., De Smedt, I., Lerot, C., Finkenzeller, H., Hendrick, F., Koenig, T.K., Lee, C.F., Knote, C., Yu, H., Van Roozendaal, M., 2020. Global nitrous acid emissions and levels of regional oxidants enhanced by wildfires. *Nature Geoscience* 13, 681-686.
- Tie, X., Long, X., Li, G., Zhao, S., Cao, J., Xu, J., 2019. Ozone enhancement due to the photodissociation of nitrous acid in eastern China. *Atmospheric Chemistry and Physics* 19, 11267-11278.
- VandenBoer, T.C., Brown, S.S., Murphy, J.G., Keene, W.C., Young, C.J., Pszenny, A.A.P., Kim, S., Warneke, C., de Gouw, J.A., Maben, J.R., Wagner, N.L., Riedel, T.P., Thornton, J.A., Wolfe, D.E., Dube, W.P., Ozturk, F., Brock, C.A., Grossberg, N., Lefer, B., Lerner, B., Middlebrook, A.M., Roberts, J.M., 2013. Understanding the role of the ground surface in HONO vertical structure: High resolution vertical profiles during NACHTT-11. *J Geophys Res-Atmos* 118, 10155-10171.
- Villena, G., Kleffmann, J., Kurtenbach, R., Wiesen, P., Lissi, E., Rubio, M.A., Croxatto, G., Rappenglück, B., 2011. Vertical gradients of HONO, NO<sub>x</sub> and O<sub>3</sub> in Santiago de Chile. *Atmospheric Environment* 45, 3867-3873.
- Wang, F., An, J.L., Li, Y., Tang, Y.J., Lin, J., Qu, Y., Chen, Y., Zhang, B., Zhai, J., 2014. Impacts of uncertainty in AVOC emissions on the summer RO<sub>x</sub> budget and ozone production rate in the three most rapidly-developing economic growth regions of China. *Advances in Atmospheric Sciences* 31, 1331-1342.
- Wang, X., Zhang, Y., Hu, Y., Zhou, W., Lu, K., Zhong, L., Zeng, L., Shao, M., Hu, M., Russell, A.G., 2010. Process analysis and sensitivity study of regional ozone formation over the Pearl River Delta, China, during the PRIDE-PRD2004 campaign using the Community Multiscale Air Quality modeling system. *Atmospheric Chemistry and Physics* 10, 4423-4437.
- Wang, Y., Apituley, A., Bais, A., Beirle, S., Benavent, N., Borovski, A., Bruchkouski, I., Chan, K.L., Donner, S., Drosoglou, T., Finkenzeller, H., Friedrich, M.M., Friess, U., Garcia-Nieto, D., Gomez-Martin, L., Hendrick, F., Hilboll, A., Jin, J.L., Johnston, P., Koenig, T.K., Kreher, K., Kumar, V., Kyuberis, A., Lampel, J., Liu, C., Liu, H.R., Ma, J.Z., Polyansky, O.L., Postlyakov, O., Querel, R., Saiz-Lopez, A., Schmitt, S., Tian, X., Tirpitz, J.L., Van Roozendaal, M., Volkamer, R., Wang, Z.R., Xie, P.H., Xing, C.Z., Xu, J., Yela, M., Zhang, C.X., Wagner, T., 2020. Inter-comparison of MAX-DOAS measurements of tropospheric HONO slant column densities and vertical profiles during the CINDI-2 campaign. *Atmospheric Measurement Techniques* 13, 5087-5116.
- Wang, Y., Dörner, S., Donner, S., Böhnke, S., De Smedt, I., Dickerson, R.R., Dong, Z., He, H., Li, Z., Li, Z., Li, D., Liu, D., Ren, X., Theys, N., Wang, Y., Wang, Y., Wang, Z., Xu, H., Xu, J., Wagner,

1546 T., 2019. Vertical profiles of NO<sub>2</sub>, SO<sub>2</sub>, HONO, HCHO, CHOCHO and aerosols derived from  
 1547 MAX-DOAS measurements at a rural site in the central western North China Plain and their  
 1548 relation to emission sources and effects of regional transport. *Atmospheric Chemistry and Physics*  
 1549 19, 5417-5449.

1550 Wilkinson, S., Mills, G., Illidge, R., Davies, W.J., 2012. How is ozone pollution reducing our food  
 1551 supply? *J Exp Bot* 63, 527-536.

1552 Wong, K.W., Oh, H.J., Lefer, B.L., Rappengluck, B., Stutz, J., 2011. Vertical profiles of nitrous acid in  
 1553 the nocturnal urban atmosphere of Houston, TX. *Atmospheric Chemistry and Physics* 11,  
 1554 3595-3609.

1555 Wong, K.W., Tsai, C., Lefer, B., Haman, C., Grossberg, N., Brune, W.H., Ren, X., Luke, W., Stutz, J.,  
 1556 2012. Daytime HONO vertical gradients during SHARP 2009 in Houston, TX. *Atmospheric*  
 1557 *Chemistry and Physics* 12, 635-652.

1558 Wu, D., Horn, M.A., Behrendt, T., Muller, S., Li, J., Cole, J.A., Xie, B., Ju, X., Li, G., Ermel, M.,  
 1559 Oswald, R., Frohlich-Nowoisky, J., Hoor, P., Hu, C., Liu, M., Andreae, M.O., Poschl, U., Cheng,  
 1560 Y., Su, H., Trebs, I., Weber, B., Sorgel, M., 2019. Soil HONO emissions at high moisture content  
 1561 are driven by microbial nitrate reduction to nitrite: tackling the HONO puzzle. *ISME J* 13,  
 1562 1688-1699.

1563 Xing, C., Liu, C., Hu, Q., Fu, Q., Wang, S., Lin, H., Zhu, Y., Wang, S., Wang, W., Javed, Z., 2021.  
 1564 Vertical distributions of wintertime atmospheric nitrogenous compounds and the corresponding  
 1565 OH radicals production in Leshan, southwest China. *Journal of Environmental Sciences* 105,  
 1566 44-55.

1567 Xing, L., Wu, J.R., Elser, M., Tong, S.R., Liu, S.X., Li, X., Liu, L., Cao, J.J., Zhou, J.M., El-Haddad, I.,  
 1568 Huang, R.J., Ge, M.F., Tie, X.X., Prevot, A.S.H., Li, G.H., 2019. Wintertime secondary organic  
 1569 aerosol formation in Beijing-Tianjin-Hebei (BTH): contributions of HONO sources and  
 1570 heterogeneous reactions. *Atmospheric Chemistry and Physics* 19, 2343-2359.

1571 Xu, J., Zhang, Y.H., Wang, W., 2006. Numerical study on the impacts of heterogeneous reactions on  
 1572 ozone formation in the Beijing urban area. *Advances in Atmospheric Sciences* 23, 605-614.

1573 Xu, W., Yang, W., Han, C., Yang, H., Xue, X., 2021. Significant influences of TiO<sub>2</sub> crystal structures on  
 1574 NO<sub>2</sub> and HONO emissions from the nitrates photolysis. *Journal of Environmental Sciences* 102,  
 1575 198-206.

1576 Xue, C., Zhang, C., Ye, C., Liu, P., Catoire, V., Krysztofiak, G., Chen, H., Ren, Y., Zhao, X., Wang, J.,  
 1577 Zhang, F., Zhang, C., Zhang, J., An, J., Wang, T., Chen, J., Kleffmann, J., Mellouki, A., Mu, Y.,  
 1578 2020. HONO Budget and Its Role in Nitrate Formation in the Rural North China Plain.  
 1579 *Environmental Science & Technology* 54, 11048-11057.

1580 Xue, C.Y., Ye, C., Zhang, C.L., Catoire, V., Liu, P.F., Gu, R.R., Zhang, J.W., Ma, Z.B., Zhao, X.X.,  
 1581 Zhang, W.Q., Ren, Y.G., Krysztofiak, G., Tong, S.R., Xue, L.K., An, J.L., Ge, M.F., Mellouki, A.,  
 1582 Mu, Y.J., 2021. Evidence for Strong HONO Emission from Fertilized Agricultural Fields and its  
 1583 Remarkable Impact on Regional O<sub>3</sub> Pollution in the Summer North China Plain. *ACS Earth Space*  
 1584 *Chem.* 5, 340-347.

1585 Yang, K., Kong, L., Tong, S., Shen, J., Chen, L., Jin, S., Wang, C., Sha, F., Wang, L., 2021a. Double  
 1586 High-Level Ozone and PM<sub>2.5</sub> Co-Pollution Episodes in Shanghai, China: Pollution Characteristics  
 1587 and Significant Role of Daytime HONO. *Atmosphere* 12, 557.

1588 Yang, W., Han, C., Yang, H., Xue, X., 2018. Significant HONO formation by the photolysis of nitrates  
 1589 in the presence of humic acids. *Environ Pollut* 243, 679-686.

Formatted: Subscript

1590 Yang, W., Han, C., Zhang, T., Tang, N., Yang, H., Xue, X., 2021b. Heterogeneous photochemical  
1591 uptake of NO<sub>2</sub> on the soil surface as an important ground-level HONO source. *Environ. Pollut.*  
1592 271, 116289.

1593 Ye, C., Gao, H., Zhang, N., Zhou, X., 2016a. Photolysis of Nitric Acid and Nitrate on Natural and  
1594 Artificial Surfaces. *Environmental Science & Technology* 50, 3530-3536.

1595 Ye, C., Zhang, N., Gao, H., Zhou, X., 2017. Photolysis of Particulate Nitrate as a Source of HONO and  
1596 NO<sub>x</sub>. *Environmental Science & Technology* 51, 6849-6856.

1597 [Ye, C., Zhou, X., Pu, D., Stutz, J., Festa, J., Spolaor, M., Cantrell, C., Mauldin, R.L., Weinheimer, A.,  
1598 Haggerty, J., 2015. Comment on “Missing gas-phase source of HONO inferred from Zeppelin  
1599 measurements in the troposphere”. \*Science\* 348, 1326-d.](#)

1600 [Ye, C., Zhou, X., Pu, D., Stutz, J., Festa, J., Spolaor, M., Tsai, C., Cantrell, C., Mauldin, R.L., 3rd,  
1601 Campos, T., Weinheimer, A., Hornbrook, R.S., Apel, E.C., Guenther, A., Kaser, L., Yuan, B., Karl,  
1602 T., Haggerty, J., Hall, S., Ullmann, K., Smith, J.N., Ortega, J., Knote, C., 2016b. Rapid cycling of  
1603 reactive nitrogen in the marine boundary layer. \*Nature\* 532, 489-491.](#)

1604 [Zaveri, R.A., Easter, R.C., Fast, J.D., Peters, L.K., 2008. Model for Simulating Aerosol Interactions  
1605 and Chemistry \(MOSAIC\). \*J Geophys Res-Atmos\* 113. doi:10.1029/2007JD008782.](#)

1606 Zhang, H.L., Li, J.Y., Ying, Q., Yu, J.Z., Wu, D., Cheng, Y., He, K.B., Jiang, J.K., 2012. Source  
1607 apportionment of PM<sub>2.5</sub> nitrate and sulfate in China using a source-oriented chemical transport  
1608 model. *Atmospheric Environment* 62, 228-242.

1609 Zhang, J., An, J., Qu, Y., Liu, X., Chen, Y., 2019a. Impacts of potential HONO sources on the  
1610 concentrations of oxidants and secondary organic aerosols in the Beijing-Tianjin-Hebei region of  
1611 China. *The Science of the total environment* 647, 836-852.

1612 Zhang, J., Chen, J., Xue, C., Chen, H., Zhang, Q., Liu, X., Mu, Y., Guo, Y., Wang, D., Chen, Y., Li, J.,  
1613 Qu, Y., An, J., 2019b. Impacts of six potential HONO sources on HO<sub>x</sub> budgets and SOA formation  
1614 during a wintertime heavy haze period in the North China Plain. *The Science of the total  
1615 environment* 681, 110-123.

1616 Zhang, J., Guo, Y., Qu, Y., Chen, Y., Yu, R., Xue, C., Yang, R., Zhang, Q., Liu, X., Mu, Y., Wang, J., Ye,  
1617 C., Zhao, H., Sun, Q., Wang, Z., An, J., 2020a. Effect of potential HONO sources on peroxyacetyl  
1618 nitrate (PAN) formation in eastern China in winter. *Journal of Environmental Sciences* 94, 81-87.

1619 Zhang, J., Ran, H., Guo, Y., Xue, C., Liu, X., Qu, Y., Sun, Y., Zhang, Q., Mu, Y., Chen, Y., Wang, J., An,  
1620 J., 2022. High crop yield losses induced by potential HONO sources — A modelling study in the  
1621 North China Plain. *Science of The Total Environment* 803, 149929.

1622 Zhang, L., Wang, T., Zhang, Q., Zheng, J.Y., Xu, Z., Lv, M.Y., 2016. Potential sources of nitrous acid  
1623 (HONO) and their impacts on ozone: A WRF-Chem study in a polluted subtropical region. *J  
1624 Geophys Res-Atmos* 121, 3645-3662.

1625 Zhang, N., Zhou, X.L., Shepson, P.B., Gao, H.L., Alaghmand, M., Stirn, B., 2009. Aircraft  
1626 measurement of HONO vertical profiles over a forested region. *Geophysical Research Letters* 36.  
1627 doi:10.1029/2009GL038999.

1628 Zhang, Q., Geng, G., 2019. Impact of clean air action on PM<sub>2.5</sub> pollution in China. *Science China Earth  
1629 Sciences* 62, 1845-1846.

1630 Zhang, S., Sarwar, G., Xing, J., Chu, B., Xue, C., Sarav, A., Ding, D., Zheng, H., Mu, Y., Duan, F., Ma,  
1631 T., He, H., 2021. Improving the representation of HONO chemistry in CMAQ and examining its  
1632 impact on haze over China. *Atmospheric Chemistry and Physics* 21, 15809-15826.

1633 Zhang, W., Tong, S., Ge, M., An, J., Shi, Z., Hou, S., Xia, K., Qu, Y., Zhang, H., Chu, B., Sun, Y., He,

Formatted: Subscript

1634 H., 2019c. Variations and sources of nitrous acid (HONO) during a severe pollution episode in  
1635 Beijing in winter 2016. *The Science of the total environment* 648, 253-262.

1636 Zhang, W.Q., Tong, S.R., Jia, C.H., Wang, L.L., Liu, B.X., Tang, G.Q., Ji, D.S., Hu, B., Liu, Z.R., Li,  
1637 W.R., Wang, Z., Liu, Y., Wang, Y.S., Ge, M.F., 2020b. Different HONO Sources for Three Layers  
1638 at the Urban Area of Beijing. *Environmental science & technology* 54, 12870-12880.

1639 [Zhao, H., Zhang, Y., Qi, Q., Zhang, H., 2021. Evaluating the Impacts of Ground-Level O<sub>3</sub> on Crops in  
1640 China. \*Current Pollution Reports\* 7, 565-578.](#)

1641 Zheng, H., Song, S., Sarwar, G., Gen, M., Wang, S., Ding, D., Chang, X., Zhang, S., Xing, J., Sun, Y.,  
1642 Ji, D., Chan, C.K., Gao, J., McElroy, M.B., 2020. Contribution of Particulate Nitrate Photolysis to  
1643 Heterogeneous Sulfate Formation for Winter Haze in China. *Environmental Science &  
1644 Technology Letters* 7, 632-638.

1645 Zhou, X., Gao, H., He, Y., Huang, G., Bertman, S.B., Civerolo, K., Schwab, J., 2003. Nitric acid  
1646 photolysis on surfaces in low-NO<sub>x</sub> environments: Significant atmospheric implications.  
1647 *Geophysical Research Letters* 30. doi:10.1029/2003GL018620.

1648 Zhu, C., Xiang, B., Zhu, L., Cole, R., 2008. Determination of absorption cross sections of  
1649 surface-adsorbed HNO<sub>3</sub> in the 290–330 nm region by Brewster angle cavity ring-down  
1650 spectroscopy. *Chemical Physics Letters* 458, 373-377.

1651 Zhu, Y.W., Liu, W.Q., Fang, J., Xie, P.H., Dou, K., Qin, M., Si, F.Q., 2011. Monitoring and Analysis of  
1652 Vertical Profile of Atmospheric HONO, NO<sub>2</sub> in Boundary Layer of Beijing. *Spectroscopy and  
1653 Spectral Analysis* 31, 1078-1082.

1654

Formatted: Subscript